November, 2024

“Location Location Location!” - The potential impact of hydrocarbon exploration in the Israeli Mediterranean on natural and socioeconomic assets

Assaf Pertzelan and Igal Berenshtein
The Department of Marine Biology, Charney School of Marine Sciences, University of Haifa

Report Prepared for and funded by:
The Society for the Protection of Nature in Israel

Abstract

The exploration and extraction of hydrocarbon resources in the Israeli Mediterranean Sea pose significant environmental and socioeconomic risks. Natural gas drilling carries the risk of hydrocarbon leaks, both from the liquid phase of the gas (also called condensate) and from crude oil which may be present in the gas field. A major risk of this activity stems from potential loss of well control, especially during the exploration drilling phase. In recent years, Israel has been substantially expanding search areas for new hydrocarbon deposits, however the different potential damages emanating from potential spills from each of these deposits was not systematically tested and is currently unknown. In this study we aim to bridge this gap, assessing the potential impact of hydrocarbon spills from six proposed exploration blocks. We use advanced oil spill modeling techniques (OpenOil and OceanDrift) to simulate multiple scenarios of medium scale events (70 tons of pollutant per scenario). By analyzing the spread of oil and the liquid phase of natural gas under various seasonal conditions, we evaluate the potential impacts posed to eleven natural and socioeconomic assets, including marine protected areas (MPAs), desalination plants, maricultural areas, beaches, estuaries, and ports. In contrast to previous studies/reports worldwide, the current study, in addition to providing pollutants transport analysis, also provides a comprehensive analysis which systematically examines and ranks the severity of various spill locations across a wide range of natural and socio-economic assets. Another unique aspect of our analysis is the consideration of meaningful benchmark pollutant concentrations, which provides information about the area and the duration of toxic (to marine

wildlife) pollutant concentrations, and the number of days during which desalination plants would not be able to operate. The results reveal that the location of the spill site, the season, and the oil type, have a marked effect on the impact of the spill on different assets. Spills originating from Zone E, particularly Block E65, have the most severe potential for damage, especially to coastal infrastructure and northern MPAs, although toxic-to-marine-wildlife concentrations of (polycyclic aromatic hydrocarbons (PAH) >1ppb) were observed for all the MPA's. The simulation also highlights the heightened risks for coastal and continental shelf assets during summer months and storm events, with crude oil posing more severe long-term impacts than liquid gas phase. Additionally, coastal desalination plants and mariculture farms are expected to face prolonged exposure to hydrocarbon concentrations that could significantly disrupt operations for up to 25 days, with potential major economic impact. As the raw results include thousands of plots and analyses, we provide a friendly user interface, which provides simple and comprehensive access to the results. Importantly, a parameter sensitivity test indicated that the overall results and conclusions remain robust and largely unchanged, especially with respect to the severity of Zone E spills on the assets. Our findings emphasize the importance of the spill location and its effects on natural and socioeconomic assets, and hence the need for robust regulatory measures—such as carrying out a robust potential impact assessment for search areas in question —to be implemented before initiating the licensing process and selection of offshore drilling zones, ensuring that risks associated with hydrocarbon development are fully addressed from the onset.

Introduction

The exploration and subsequent discoveries of natural gas reserves in the Israeli Mediterranean have reshaped the energy dynamics of the region. The foundational discoveries of the Tamar field in 2009 and the Leviathan field in 2010 are repeatedly highlighted in the literature as pivotal moments in the region's energy exploration history (Needham et al., 2017; Karcz et al., 2019). These fields, along with others such as Dalit and Aphrodite, have significantly contributed to the area being recognized for its hydrocarbon potential, and has enhanced energy security and economic growth through domestic supply stabilization and strategic export agreements (Khosla, 2020).

However, natural gas production also poses serious risks to the marine environment, and to coastal and marine natural and socioeconomic resources. Oil and gas explorations can lead to habitat destruction, pollution, and disturbances to marine life, threatening the biodiversity of this fragile ecosystem. Additionally, the coastal and marine resources that communities depend on for livelihoods, tourism, and cultural value may be adversely affected. Therefore, it is crucial to balance the exploitation of these resources with stringent environmental safeguards to preserve the marine environment and its natural and socioeconomic assets.

In natural gas explorations within the Israeli Mediterranean marine environment, three primary pollutants are of concern: natural gas, oil, and liquid gas phase. Natural gas mainly consists of methane, while oil, though less common, can be released during extraction, transport, or spills, causing chronic pollution and toxic effects on marine life (Cordes et al., 2016). Natural gas production poses significant risks to marine ecosystems and coastal resources. The extraction process can lead to habitat destruction, pollution, and disturbances to marine life, threatening biodiversity in these sensitive environments (Cordes et al., 2016). For example, early life stages of speckled seatrout (*Cynoscion nebulosus*) exposed to hydrocarbons pollution under natural light conditions for 24 h results in LC_{50} of 0.18 (Alloy et al., 2017).

The impacts extend beyond wildlife to affect coastal communities. Regular emissions from oil and gas operations result in chronic pollution of marine environments, impairing ecosystem functioning (Cordes et al., 2016). This can adversely affect livelihoods dependent on fishing, tourism, and other marine-based industries (Solo-Gabriele et al., 2021). Large-scale offshore projects release substantial pollutants into the atmosphere and water, with environmental consequences persisting long after production ceases (Deepwater Horizon Natural Resource Damage Assessment Trustees et al., 2017).

Deep-sea (depth $\geq$ 1000 m) oil and gas spills pose significant challenges, affecting both marine ecosystems and socioeconomic assets. The long-term ecological consequences include alterations in biodiversity and species composition, as evidenced by research on the Deepwater Horizon oil spill (Barron, 2012). Hence, these impacts have obvious relevance for the possible effects of hydrocarbon spills on MPAs, which are the “banks” and the “insurance policies” of our marine ecosystems (Sala and Giakoumi, 2018). Hydrocarbons spills also affect industrial sectors dependent on seawater, such as desalination plants and power stations (Nichols and Parker, 1989). Additionally, such pollution events can cover vast coastal areas, impacting the beaches

and other coastal assets, impacting human health, economy, and coastal population resilience (Solo-Gabriele et al., 2021).

Despite the documented severe impacts that hydrocarbons pollution has on natural and socioeconomic assets, these impacts are rarely comprehensively assessed both in retrospect and in terms of potential impact assessment of possible spill scenarios (Nelson et al., 2015). In the context of the Israeli Mediterranean oil and gas exploration and extraction, previous works assessed the possible hydrocarbon transport dynamics under various scenarios (e.g., Brenner, 2015; Goldman et al., 2015). However, these were limited in their spatial extents, and were not extended to examinations of how natural and socioeconomic assets may be affected by these spills.

In the current report, we bridge this gap, using as a case study the realistic potential gas exploration regions that were marketed in the fourth gas exploration tender. Specifically, we use oil fate and transport models to simulate multiple scenarios of hydrocarbon pollution from six blocks that are proposed for hydrocarbon exploration. We analyze the possible impacts on eleven different natural and socioeconomic assets including desalination plants, mariculture, MPAs, beaches, estuaries, and ports.

Methods

Goal and scope definition

Given the limited representation of spatial variability in spill extent and impact from proposed hydrocarbon exploration areas in the current permitting pipeline, it is crucial to assess the variability of spill impacts in exploratory drilling, with a focus on spill locations and their effects on selected asset groups (Figure 1). Subsequently, an Advisory Steering Committee was assembled to represent diverse stakeholder interests, review, and confirm the aims and scope of the project.

Asset Groups Examined

We analyzed various asset groups to assess their ecological, economic, and infrastructural importance and their vulnerability to hydrocarbon spill contamination. Each group includes specific assets essential to maintaining ecosystem health, public services, or community

resources. Polygons spatial data was provided by the Society for the Protection of Nature in Israel, which was acquired as part of the Offshore Oil and Gas Exploration and Production Strategic Environmental Assessment (SEA) (Geo-prospect Ltd., 2016).

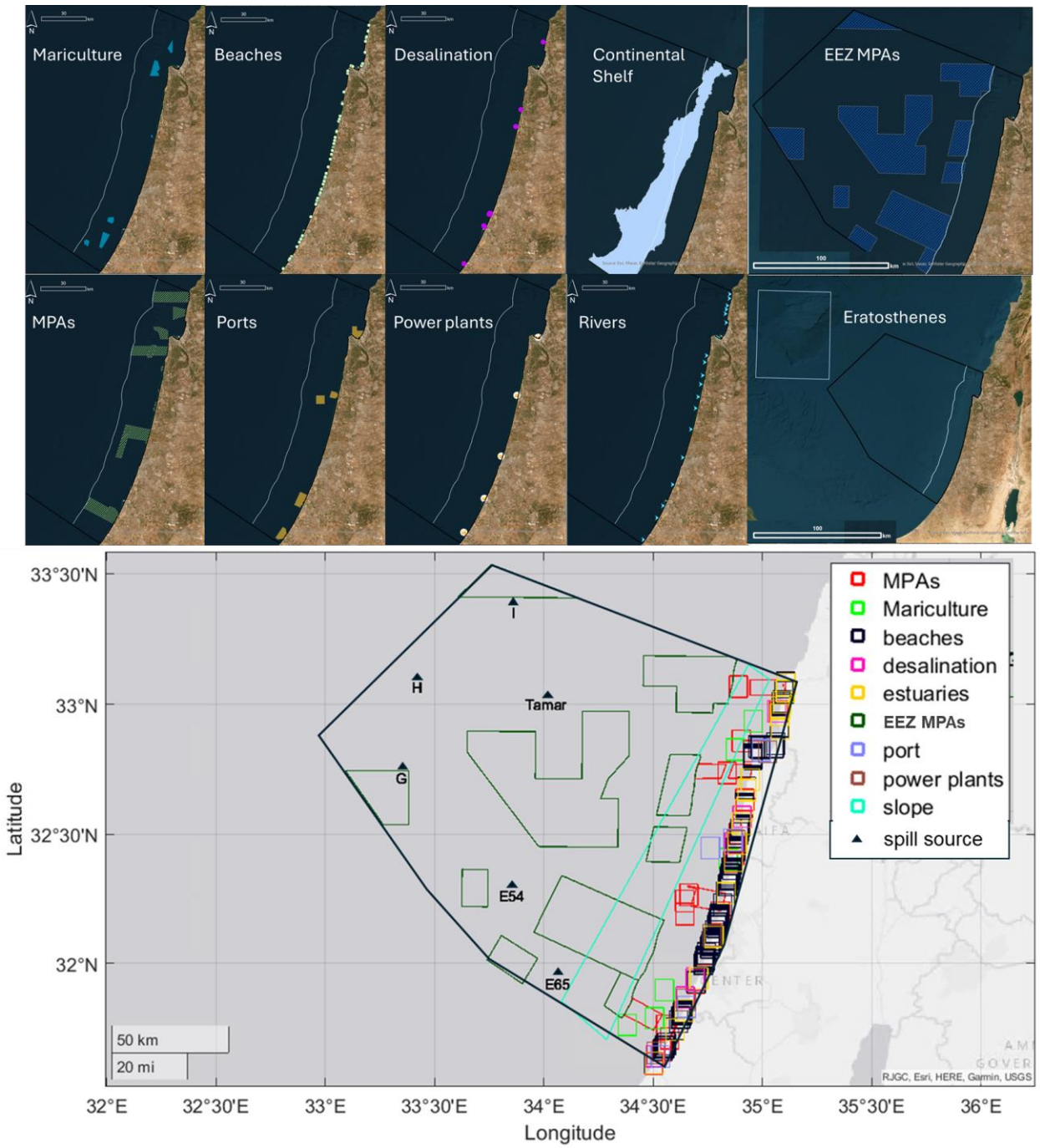

Figure 1. A map of all the different assets groups and the spill sites.

Marine Protected Areas (MPAs)

Marine Protected Areas (MPAs) are crucial for maintaining the health and resilience of marine ecosystems, providing a wide array of ecosystem services. They serve as vital nurseries for many

species, support biodiversity by protecting habitats, and enhance fisheries productivity through spillover effects into adjacent areas. MPAs also contribute to carbon sequestration, protect coastal communities from erosion, and support tourism and recreation. However, these vital ecosystem services are severely threatened by large hydrocarbon spills. Oil and gas can directly smother benthic habitats, kill marine life through toxicity, and disrupt food webs. The long-term effects of hydrocarbons on water quality and sediment can damage sensitive ecosystems within MPAs, potentially causing irreversible damage to biodiversity and impairing the ability of MPAs to provide their valuable ecosystem services for many decades. The economic consequences of such damage to fisheries, tourism, and other MPA-related industries can also be substantial. The presence of MPAs in hydrocarbon exploration areas therefore highlights the need for comprehensive risk assessments and stringent preventative measures before any exploration or extraction activities commence (Palumbi, 2001).

Based on the sensitivity of marine wildlife to hydrocarbon pollution, a toxic threshold for hydrocarbon concentration in both mariculture areas and MPAs is a PAH concentration of 1 ppb, representing the toxic-to-marine-life threshold, especially in the context of early life stages of fish and invertebrates(Deepwater Horizon Natural Resource Damage Assessment Trustees et al., 2017).

MPAs are categorized into two types based on depth and location: Continental Shelf MPAs and Deep Sea MPAs. Continental Shelf MPAs (north to south): Iyye Hof Rosh Ha-Niqra, Yam Atlit, Yam Rosh Haniqra – Akhziv, Yam Shave-Ziyyon Bustan Ha-Galil, Yam Rosh Karmel, Shiqmona, Yam Atlit - Rekhes Amok, , Yam Dor Ha-Bonim, Iyye Hof Dor U-Ma'agan Mikha'el, Yam Jisr Ez-zarqa, AkhzivYam-Qesarya, Yam Gador (harhava), Yam Gador, Yam Mikhmoret, Yam Poleg, Yam Apoloniya, Yafo-Givat Aliya, Yam Palmahim, Yam Evtah, Yamit Evtah Darom, Holot Nizzanim (harhava),Yam Ashqelon, Yam Shiqma,
Deep sea/ Israeli Exlussive Economic Zone (EEZ) MPAs include: North Levant Channel, Sediment Waves, Heart of the Sea, Dor Slide Base, Patropoda Skeletons, Slope Center, Southern Springs, Palmahim Disturbance, Southern Fan, Southern Slides.

Mariculture

Mariculture areas are essential for sustainable aquaculture, contributing to food security and local economies. These areas are vulnerable to hydrocarbon contamination, which can lead to

substantial ecological and economic losses. Mariculture facilities, vital for food production and economies, are extremely vulnerable to hydrocarbon spills. Oil contamination directly harms cultured species, fouls equipment, and disrupts operations, causing economic losses. Long-term water quality impacts also threaten the health of the surrounding ecosystem and the sustainability of mariculture. Here too, the toxic threshold was set for a PAH concentration of 1 ppb, representing the toxic-to-marine-life threshold, especially to early life stages of fish and invertebrates (Deepwater Horizon Natural Resource Damage Assessment Trustees et al., 2017). Assets (north to south): Acre, license; Haifa, license; Ashkelon, exist; Hadera, exist; Ashdod, license; Ashdod, potential (Figure 1).

Desalination stations

Coastal desalination plants, crucial for freshwater supply, are vulnerable to hydrocarbon spills. Oil contamination can directly damage systems' intake, fouling membranes and requiring costly cleaning and repairs. Disrupted operations lead to freshwater shortages, impacting human populations and economies. Hydrocarbon contamination can also affect the quality of the treated water, potentially requiring additional treatment steps and further increasing costs. A hydrocarbon concentration of 500 ppb represents the threshold above which desalination plants can no longer operate properly. The proximity of desalination plants to potential spill sources necessitates robust risk assessment and preventative measures to ensure continued reliable operation (Ogunbiyi et al., 2023). Assets (north to south): Western Galilee, Maagan Michael, Hadera, Soreq, Palmachim, Ashdod, Ashkelon (Figure 1)

Ports

Ports, vital for international trade and economic activity, are vulnerable to the impacts of hydrocarbon spills. Oil contamination can directly damage port infrastructure, including docks, terminals, and equipment, necessitating costly repairs and potentially causing significant operational disruptions. Spills can also impede shipping activities, leading to delays, cargo damage, and economic losses. Furthermore, the cleanup process itself can disrupt port operations for extended periods. The potential for long-term damage to ports, further impacting economic activities, necessitates comprehensive risk assessment and mitigation strategies for ports located

near hydrocarbon exploration or transportation routes. Assets (north to south): Haifa, Hadera, Gatan, Ashdod, Ashkelon (Figure 1).

Power Plants

Coastal power plants, essential for energy production, are vulnerable to hydrocarbon spills. Oil contamination can directly damage intake systems, crucial for cooling operations, potentially leading to plant shutdowns and significant power outages. The resulting energy shortages can have wide-ranging economic and social consequences. Cleanup and repair efforts following a spill can also cause prolonged disruptions to power generation. The potential for long-term environmental damage to sensitive ecosystems surrounding the plant necessitates careful consideration of spill risks during the siting and operation of coastal power plants.
Assets (north to south): Haifa, Hadera, Reading, Ashdod, Ashkelon (Figure1).

Beaches

Beaches, vital recreational and ecological resources, are highly vulnerable to the devastating impacts of hydrocarbon spills. Oil contamination renders beaches unusable for recreation, harming tourism and local economies, impacting numerous touristic assets located on or near the beach. The cleanup process is lengthy, expensive, and often incomplete, leaving lingering impacts on aesthetics and water quality. Oil and gas can also smother intertidal ecosystems, harming sensitive species and disrupting ecological processes. The long-term effects of hydrocarbon contamination on sediment and water quality can severely impact beach health and functionality, necessitating comprehensive cleanup and restoration efforts.
Assets (north to south): Betzet Beach, Achziv Park Beach, Achziv Beach - Southern Station, Separate Beach Section 1, Separate Beach Section 2, Gali Galil Beach, Sokolov, Shavei Zion Beach, Argaman Beach, Tamarim Beach, Zebulun Beach, Kiryat Haim Beach - Station No. 1, Bat Galim, Kiryat Haim Beach - Station No. 2, Kiryat Haim Beach - Station No. 3, The Quiet Beach, Carmel Beach - Northern Station, Carmel Beach - Southern Station, Dado-Zamir Beach - Station No. 1, Dado-Zamir Beach - Station No. 2, Dado-Zamir Beach - Station No. 3, Dado-Zamir Beach - Station No. 4, Dado-Zamir Beach - Station No. 5, Neve Yam Beach, Dor Beach - Station No. 1, Dor Beach - Station No. 2, Dor Beach - Station No. 3, Jisr, Aqueduct Beach, Caesarea Port, Sea Village, Givat Olga Separate Beach, Givat Olga Central Beach, Givat Olga

Southern Beach, Mikhmoret - Station No. 1, Mikhmoret - Station No. 2, Beit Yanai, Neurim Beach, Kiryat Sanz, HaOnot Beach, Amphi Beach, Herzl, Sironit A Beach, Sirionit B Beach, Argaman Beach, Poleg Beach, Shefayim-Ga'ash, Nof Yam, HaSharon, Zebulun, Arcadia North Beach, Arcadia Center Beach, Arcadia South Beach - Disabled, Separate Beach, Cliff Beach - Station No. 1, Cliff Beach - Station No. 2, Tel Baruch Beach - Station No. 1, Nordau Beach (Metzitzim), Nordau Separate Beach, Hilton North, Gordon, Frishman, Bograshov, Allenby (Jerusalem), Aviv Beach, Charles Clore, Jaffa-Givat Aliya, Jerusalem, HaSela - Station No. 1, HaSela - Station No. 2, HaSela - Station No. 3, Example Beach, The Riviera, Separate Beach, Tayo, Rishon LeZion Beach - Station No. 4, Rishon LeZion Beach - Station No. 3, Rishon LeZion Beach - Station No. 2, Rishon LeZion Beach - Station No. 1, Palmachim Beach, Mei Ami Beach, Lido, Oranim, Arches Beach, Quarter Ya, Riviera, Nitzanim, Bar Kochva, Delilah, Ashkelon National Park Beach, Zikim (Figure1).

.

Estuaries

Estuaries play a crucial role in the environment, particularly for early life stages of various species. These dynamic ecosystems serve as vital nurseries for many marine and aquatic species, providing a rich supply of nutrients, shelter, and breeding grounds (Tom and Galil, 1991). The brackish water found in estuaries supports a diverse range of organisms, from juvenile fish to crustaceans, which rely on these habitats for survival and growth. The complex structure of estuarine environments offers a sanctuary where young organisms can find refuge from predators and harsh oceanic conditions. Additionally, the high productivity of estuaries enhances food availability, crucial for the development and sustenance of young life stages, thus contributing significantly to maintaining biodiversity and supporting fisheries that humans and wildlife depend on. In addition, reduced freshwater flows from river management have intensified hypersalinity and nutrient loading, threatening native taxa(Spanier and Zviely, 2022). Estuaries are highly sensitive to hydrocarbon spills, which can harm wildlife and affect water quality (Tom and Galil, 1991). Estuaries (north to south): Betzet, Kziv, Ga'aton, Beit HaEmek, Yasaf, Na'aman, Kishon, Oren, Me'arot, Dalia, Taninim, Hadera, Alexander, Poleg, Yarkon, Sorek, Lachish, Avtach, Shikma (Figure1).

Continental Slope

The Continental Slope represents an overarching region that spans much of the continental slope, offering a comprehensive perspective on the area as a whole. It is an essential geological feature, supporting various ecological habitats that contribute to marine biodiversity. The continental slope is an essential component of marine ecosystems, playing a critical role in the early life stages of various marine species. This transitional zone between continental shelves and the deep ocean basin is characterized by its steep gradient and complex topography, offering a range of habitats that support diverse marine life. The continental slope is particularly important for the larvae and juveniles of many species, providing a habitat rich in nutrients and organic material due to its proximity to nutrient upwelling and ocean currents. These conditions create an environment where young marine organisms can thrive, finding both food and refuge from predators. Additionally, the slope's varied landscape, including submarine canyons and ridges, offers unique ecological niches that help sustain biodiversity. By supporting these early life stages, the continental slope contributes to the overall productivity and resilience of marine ecosystems, underscoring the need for its conservation. This region is highly sensitive to oil spills, as contamination could disrupt geological formations and impact the health of interconnected ecosystems.

Eratosthenes

The Eratosthenes Seamount is a significant feature of marine ecosystems, particularly for the early life stages of various marine species. The complex topography of the seamount, characterized by steep slopes, cliffs, and unique geological formations, provides a range of habitats that support diverse marine life. The elevation of the seamount encourages water currents that bring essential nutrients and organic material from the open ocean, creating an environment rich in food sources. This nutrient availability makes the seamount an ideal nursery for larvae and juvenile fish, allowing them to find shelter and avoid predators in the rocky structures and crevices.

In the Eratosthenes Seamount, diverse pelagic and meiofaunal assemblages and sessile organisms like stony corals and sponges on its hard substrates were found (Danovaro et al., 2010; Morato et al., 2010, 2012). These findings are important, as global studies indicate that cold-water coral ecosystems, such as those comprising *Lophelia pertusa* and *Madrepora oculata*,

along with sponge-dominated habitats, often shape benthic communities(Morato et al., 2012). The Eratosthenes Seamount plays a crucial role in maintaining biodiversity, which is essential for the health of marine ecosystems and contributes to the overall productivity and resilience of oceanic environments (Figure 1).

Current generation

The currents were generated based on a nested model, with Copernicus Marine Environment Monitoring Service (CMEMS) Mediterranean Monitoring and Forecasting Centre (MED MFC) physical multiyear product of the Mediterranean Sea Physics Reanalysis (Escudier et al., 2020) as the outer model, and South Eastern Levantine Israeli Prediction System (SELIPS) as the inner model. We used four years of currents data (2017-2020) as this was the limitation of the maximum available for us under the limitations for the SELIPS currents.

The CMEMS currents are based on hydrodynamic model currents output implemented over the Mediterranean Basin with a horizontal grid resolution of 1/24˚ (~ 4 km) and have 141 vertical levels, with a daily output frequency. The hydrodynamics of CMEMS are supplied by the Nucleus for European Modelling of the Ocean (NEMO; Clementi et al., 2016). The model includes data assimilation schemes (OceanVAR) of temperature and salinity vertical profiles, as well as those of satellite Sea Level Anomaly observations (Escudier *et al.*, 2020)

SELIPS is a sub-regional high resolution circulation model operated by Israel Oceanographic and Limnological Research (IOLR) that generates daily forecasts of temperature, salinity, and sea currents in the southeastern region of the Levantine basin. The oceanic general model used to run SELIPS is the Princeton Ocean Model (POM) ; Blumberg and Mellor, 1987). The resolution is 0.01ºx0.00833º (about 1 km) with 27 sigma levels, and the minimal depth is 5 meters. Initial and boundary conditions of temperature, salinity, and water velocity are taken from ALERMO forecast system (Zafirakou-Koulouris et al., 2012). Output frequency was every three hours, which were averaged to produce daily resolution currents for the hydrocarbon transport model.

Atmospheric fluxes of heat, fresh water, and momentum at the sea surface are computed from bulk formulas using the conditions taken from SKIRON, a regional atmospheric model forecast, including air temperature, specific humidity, air pressure, wind, total cloud cover and precipitation. Modeled heat flux was corrected using the remotely sensed sea surface temperature

(SST) fields taken from Copernicus Marine Service (nudging process; Nardelli et al., 2004). The validation of SELIPS model was carried out against in-situ measurements of temperature, salinity, and currents direction and velocity from Ashkelon, Hadera, and DEEPLEV mooring (see Annex 1 and (Berenshtein et al., 2024)).

We focused on four years: 2017-2020 as this was the available duration for SELIPS model runs. These years are characterized by notable variability in temperature, salinity, and currents. Inter-annual variations in these parameters, especially between 2017 and 2020, a period marked by unprecedented warming, reduced vertical mixing, and intensified stratification. High-resolution observational datasets from Israeli coastal stations (Ozer et al., 2022a; Ben-Ezra et al., 2024) and basin-wide monitoring (Ozer et al., 2022b) provided direct evidence for inter-annual warming and salinification, with robust linkages to atmospheric and mesoscale dynamics. For instance, during 2017–2020, temperature and salinity trends (warming ~0.048°C/year; salinification ~0.006/year) were identified, and temperature anomalies in 2018–2019 (~0.7°C above earlier peaks) were attributed to atmospheric anomalies and reduced freshwater fluxes (Ozer *et al.*, 2022a). Reduced vertical mixing during the study period exacerbated oxygen depletion and nutrient limitation in the photic zone, particularly in 2020–2021, intensifying oligotrophic conditions (Ben-Ezra et al., 2024).

Data Conversion to OpenDrift-Compatible Format

For the nested model we were running in Opendrift we developed two MATLAB classes ConvertHighRes and ConvertLowRes to convert high and low resolution oceanographic data into a format compatible with OpenDrift for running 42-day scenarios. The ocean current data conversion process comprised seven steps. First, the process was initialized by specifying the source and destination folders. Source data consisted of daily NetCDF (.nc) files (analysis.yyyymmdd.nc) containing variables such as longitude (lon), latitude (lat), depth (sigma), time (time), u and v velocity components, temperature, and salinity. Wind data (10 m above sea level), copied from a separate source folder, was restructured to conform to OpenDrift naming conventions (x_wind and y_wind in WindData.nc). The source of the numerical wind data is the European Centre for Medium-Range Weather Forecasts (ECMWF), and the spatial resolution of the wind model is half a degree, with a daily temporal resolution.

Next, a new NetCDF file was created to store the processed ocean current data, spanning the scenario's start date (dateStart) and duration (42 days). Note that we simulate a spill, i.e., daily release of hydrocarbons from the pollution site, during the first 14 days while the subsequent 28 days are used for tracking the spilled oil in the sea. The relevant daily source files were identified, and the file structure, including dimensions (longitude, latitude, depth, time), metadata, and variable definitions (lon, lat, depth, time, h, salinity, temperature, u, v) were established using the NetCDF4 format.

Subsequently, the depth variables, initially in sigma coordinates, were converted to z-coordinates at the specified intervals using a sigma-to-depth transformation. This transformation was applied consistently across all time steps and spatial coordinates. Finally, the daily source data were read, processed to match the standardized depth levels, and written to the newly created NetCDF file, populating fields for latitude, longitude, sea floor depth, salinity, temperature, and velocity. A quality control check was performed to confirm the presence of all required days and to verify the integrity of the data by examining minimum and maximum values for key variables.

This conversion process enabled the seamless use of the high and the low-resolution ocean current data within OpenDrift, allowing us to simulate 42-day oceanographic scenarios with accurate, high-resolution environmental forcing and lower resolution for coverage of wider area. Storm events were chosen as the multi-day events that contained winds higher than 30 knots (in the Israeli EEZ area) sorted according to their maximal duration, choosing the highest four events. The modeled storm spills started three days prior to the beginning of the storm, to capture the dynamics of the spill during storm from the beginning through the end of the storm event, and past the end of the storm with the following storm starting dates: 2017/01/24, 2019/02/02, 2019/01/11, 2020/03/14.

Simulation of drifting particles

In this study, we utilized the OpenOil and OceanDrift models from the OpenDrift simulation framework to investigate oil spills and the dispersion of marine-snow-like particles in marine environments. The simulation addressed multiple spill sites characterized by distinct geographical locations and varied depths.

The first step involved the selection of spill sites, where six different locations were identified using a named tuple (SpillSite). Each site was detailed with its corresponding name, longitude, latitude, and depth (z), as depicted in Figure 1. The sites included E54 (33.8529° E, 32.2637° N, -700 m depth), E65 (34.063029° E, 31.923470° N, -700 m depth), Site H (33.419625° E, 33.066910° N, -1300 m depth), Site I (33.860217° E, 33.353644° N, -1600 m depth), Site G (33.346193° E, 32.717234° N, -1050 m depth), and Site Tamar (34.010577° E, 33.000471° N, -1350 m depth). The release depth is 300 m above bottom depth, representing the approximate depth of separation of hydrocarbon droplets and their partitioning to the different sizes of droplets, with buoyancy and ascending speed dependent on the droplet size(Paris et al., 2012).

Subsequently, the input data required for the simulations was collated. This included a netCDF file containing wind data (WindData.nc), as well as multiple high-resolution and low-resolution netCDF files with ocean current information. These files were processed using the reader_netCDF_CF_generic from OpenDrift. The main simulation involved two types of oils: ERAWAN CONDENSATE', SHELL OIL, representing the liquid phase of natural gas, and GENERIC MEDIUM CRUDE, which represented crude oil. We simulated additional types of oil and liquid phase of natural gas in a sensitivity test (see Annex 2). These types were chosen as the specific types present in the Israeli Mediterranean wells have not been categorized and named yet. In the context of our analysis, the exact type has little relevance, as the spatial extents of the spills are very similar between crude oil and liquid gas phase (see figures 3-8).

The oil spill simulation employed the OpenOil model to simulate scenarios over a 42-day period (14 days of release and additional 28 days of tracking the pollution over time and space). OpenOil, part of the OpenDrift framework, serves as a comprehensive model for simulating oil spills and incorporates a variety of parameterizations to accurately depict oil transport and weathering processes. The model's initialization incorporated both high-resolution and low-resolution ocean current data, as well as wind data. Each spill event involved the release of 3,000 oil droplets with sizes ranging from a minimum of 1e-6 m to a maximum of 0.0005 m, configured via the set_config method to ensure realistic vertical mixing and subsea droplet distribution. Droplet seeding at each spill site covered a radius of 50 m. The release depth is 300 m above bottom depth, representing the approximate depth of separation of hydrocarbon droplets and their partitioning to the different sizes of droplets (Paris et al., 2012).

During the 14 days of pollution, the system released 214 hydrocarbon sub-pollutants daily, cumulatively amounting to 0.9 × 70 tons of hydrocarbons. This distribution reflects the modeling approach, where 90% of the pollution mass was simulated using the OpenOil platform, while the remaining 10% was modeled as marine snow using OpenDrift. The daily release of hydrocarbons was calculated to be 4.5 tons (4500 kg), with each day of release (spill) accounting for approximately 21 kg of hydrocarbons.

The parameterizations in OpenOil are critical for understanding the behavior of oil spills in different environmental contexts and include processes related to transport, oil properties, weathering, and additional relevant parameters. The model addresses transport processes through horizontal and vertical mechanisms. Horizontal transport is influenced by environmental factors such as ocean currents, wind, and Stokes drift. Additionally, it employs a random walk approach to account for diffusion resulting from unresolved turbulence.

Oil density is sourced from the NOAA database when utilizing the NOAA weathering model, and it may vary throughout the simulation due to weathering effects. In terms of weathering processes, OpenOil manages several elements of oil behavior under various conditions. Dispersion is controlled via a specific parameter, which effectively removes oil from the simulation if it becomes entrained as very small droplets. Evaporation, relevant for surface oil, can also be enabled through a designated parameter, while emulsification is handled through another specific setting. Lastly, OpenOil provides additional parameters to enhance simulation accuracy. The oil release rate can be specified using an adjustable parameter, and the wind drift factor is set to 3% of the wind speed.

Following the oil spill simulation, the OceanDrift model was employed to simulate the distribution of marine snow-like particles, informed by the outcomes of the initial oil spill simulations. The snow particles were sampled from the computed positions of the oil droplets, with a random selection of indices determining their positions. These particles were then introduced into the OceanDrift model with a terminal velocity of -100 m/day (Ross et al., 2021) and were subject to the same ocean conditions as in the oil spill simulations. Note that out of the 70 ton released, 90% (63 ton) represents the regular hydrocarbon spill simulation, and 10% (7 ton) represents the marine snow simulations.

Post processing spatial analysis

In our analysis, we evaluated a comprehensive set of metrics across 144 distinct scenarios, which were derived from combinations of 12 time points, 6 spill sites, and 2 types of oil. For every asset within each group, we calculated several key metrics that provide insights into the impact of oil spills on these assets.

The first metric calculated was the total oil mass, measured in kilograms, which represents the cumulative amount of oil present within the confines of the asset polygon. This metric allows us to assess the overall impact of the oil spill on the specific area in question. Additionally, we computed the maximal mass, also in kilograms, which denotes the peak oil mass recorded within the asset polygon over the duration of a given scenario. This metric highlights the maximum load of oil experienced at a specific point in time.

Another crucial parameter was the stranded mass, again measured in kilograms, which accounts for the total mass of oil that reached the coastline or seafloor within the asset polygon. This metric is critical for understanding the direct impact on coastal and benthic environments. We also measured the maximal concentration of total hydrocarbons, expressed in parts per billion (ppb), to identify the highest concentration level detected within the asset polygon during the scenarios.

The days of exposure metric, measured in days, was determined by counting the number of days an asset was exposed to hydrocarbon concentrations above certain thresholds. For total hydrocarbons, we set these thresholds at 50 ppb (equivalent to PAH concentration of ~1 ppb) and 500 ppb to indicate moderate and severe exposure levels, respectively. Regarding toxic polycyclic aromatic hydrocarbons (PAHs) in the water column, we used thresholds of 1 ppb, representing levels that cause significant larval mortality. The examinations of the spatial extent of the spill with respect to specific threshold is informative for various assets. For example, oil concentrations of roughly 1000 ppb at the surface are concentrations above which visible slicks tend to form (Berenshtein et al., 2020a); concentrations above 500 ppb represent the threshold above which desalination plants can no longer function (Ogunbiyi et al., 2023). Oil concentrations of approximately 50 ppb represent roughly the threshold above which oil becomes toxic to marine life (Berenshtein et al., 2020a). And oil concentrations of approximately 1 ppb represent above background concentrations levels(Wade et al., 2016).

For very small or point-source assets, such as specific beaches or power plants, we utilized a polygon with dimensions of 1×1 km around the asset. This approach was based on the premise that if oil has reached this proximity, it is likely to affect the asset. These point-source polygons, while small, might not always exhibit pollution due to their limited size. Nonetheless, they were considered essential for ensuring a comprehensive assessment of potential impacts.

Data visualization

To effectively capture and convey the intricate patterns present in our data, we employed a diverse array of visualization techniques that balance detail with clarity. These methods include the following:

Visual Geographical Maps: We utilize geographical maps to present various metrics and asset groups, employing color-coding for assets and drawing lines between spill sites and their associated asset areas. The thickness of these lines represents the mean value of the metric for each asset based on spills from a specific site. Thicker lines indicate a stronger potential impact on the corresponding asset, while thinner lines show lesser potential effects. This approach allows for clear and straightforward comparisons across all site-asset pairs, enhancing the understanding of spatial relationships and potential impacts.

Detailed Scatter Plots: We employed scatter plots for each asset group and metric to analyze scenario-specific data. Each plot organizes results by spill site, with data points color-coded by asset for consistency with map colors. Seasonal contexts were represented by different shapes: round markers for summer, diamond markers for winter, and star markers for storm events. Medium crude oil scenarios used filled markers, while liquid gas phase scenarios used empty markers. This visualization effectively highlights trends, such as high-mass scenarios from specific spill sites under certain conditions, and reveals gaps where certain spill sources may not affect particular assets. This facilitates clear interpretations of the spatial and quantitative relationships between spills and their impacts on assets.

Bar Plots by Asset: We utilized stacked bar plots for each asset group to present data in a simplified manner, arranged by latitude. These plots facilitate concise comparisons of

contributions from each spill site across various metrics, although they do not differentiate by oil type or season.

Connectivity Matrices: Connectivity matrices are used to compare the effects of different spill sites in greater detail than stacked bar plots. These matrices provide a comprehensive view of the data, revealing patterns that may not be easily discernible in other visual formats. For instance, while the average impact of each spill site may appear subtle, the matrices enhance the detection of specific trends, such as variations in contributions to different areas. This matrix format can also be applied for ranking various asset groups across all spill sites, allowing for a clearer understanding of interactions and impacts within the dataset.

Individual Scenario Plots: For each scenario, detailed density maps are utilized to illustrate cumulative spill concentrations. Additionally, maps are created to show the number of days each asset was exposed to concentrations exceeding defined thresholds for both total hydrocarbons and toxic PAH components. This approach allows for a clear visualization of exposure dynamics across different scenarios.

Results

In this section, we present the key findings from our analysis of various oil spill scenarios, focusing on the impact on different economic and environmental assets. The assets examined include ports, desalination stations, power plants, maricultural areas, estuaries, beaches, and marine protected areas. Due to the large number of scenarios and results, for the convenience of the reader, stakeholder, or concerned citizen, we have provided a user-friendly Graphical User Interface (GUI) summarizing the results.

To provide an overview, we summarized the results in a **ranking matrix** (Berenshtein et al., 2020b), which ranks the asset groups based on their vulnerability to spills from the different spill sites, aggregating data across all scenarios while disregarding seasonal and oil type variations. A clear strong impact of block E is observed on the coastal assets. Note that such average ranking captures the overall pattern, but we provide a more detailed view for a more comprehensive assessment of the different potential impacts.

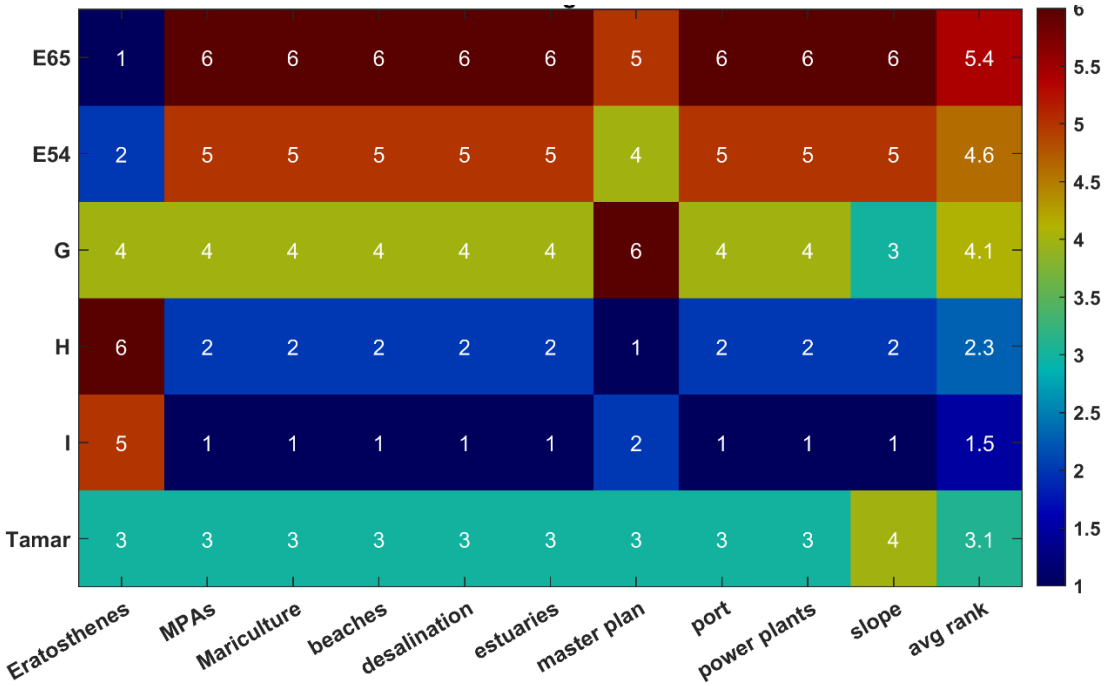

Figure 2 An overall summary of the effects of the different spill sites on the different assets, ranked by the average oil mass reaching the different assets' polygons.

Variability among scenarios

The different scenarios exhibit variability, though some general patterns can be observed. During summer months, the spatial extent of the hydrocarbon plume consistently extends toward the northeast, showing a degree of similarity across summers. In contrast, during winter months and storm conditions, the drift patterns become more circular, while slightly more dispersed on storm conditions. The location of the spill also significantly influences the drift pattern and the relevant assets at risk. Notably, in Block E, hydrocarbon spills during the summer tend to drift towards the Haifa region (Figures 3-8).

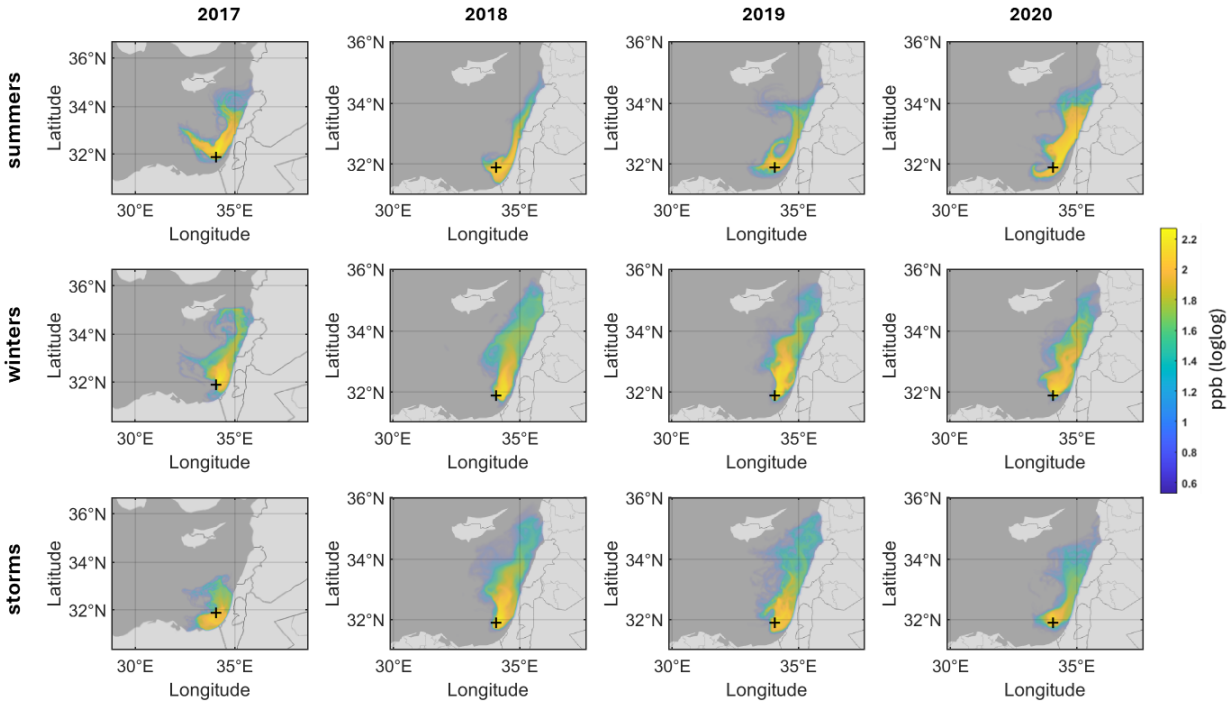

Figure 3 Total hydrocarbon concentration (ppb loglog transformed) in liquid gas phase spills from Block E zone 65 for the 12 different scenarios. The figures show variability among scenarios but similar trends within seasons, as well as variability comparing to the other spill sources. The four panel columns represent the four simulation years 2017-2020 (from left to right).

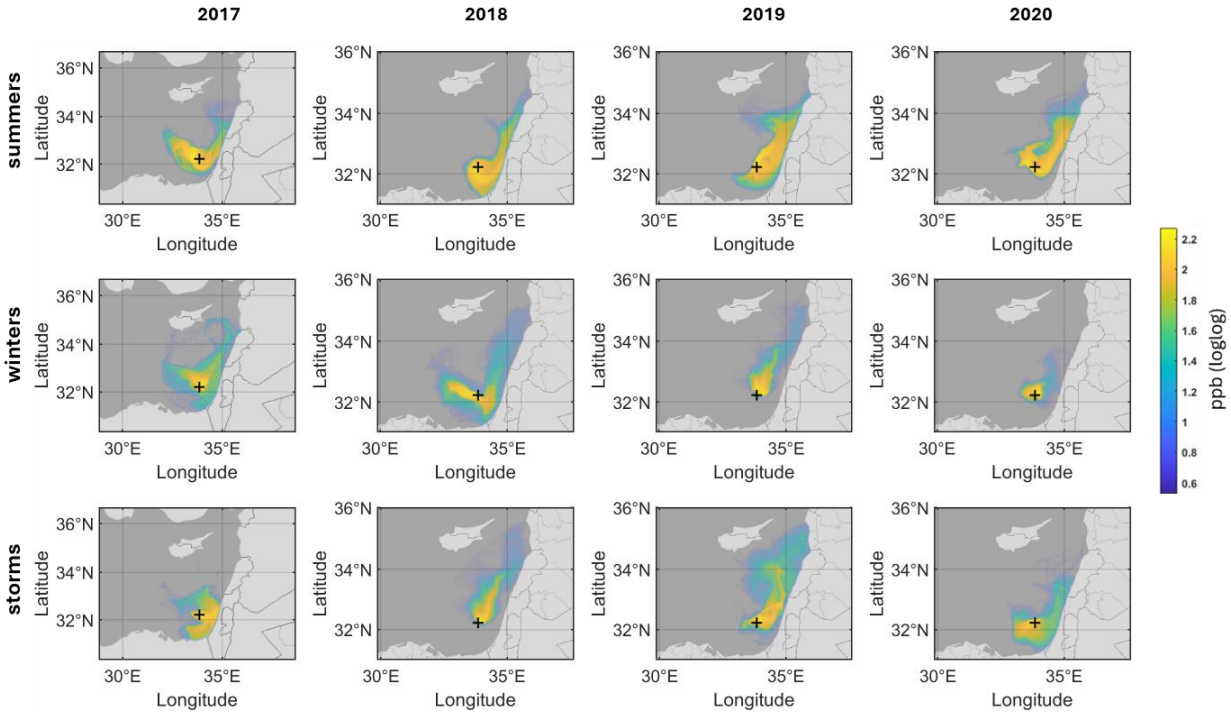

Figure 4 Total hydrocarbon concentration (ppb loglog transformed) in liquid gas phase spills from Block E zone 54 for the 12 different scenarios. The four panel columns represent the four simulation years 2017-2020 (from left to right).

.

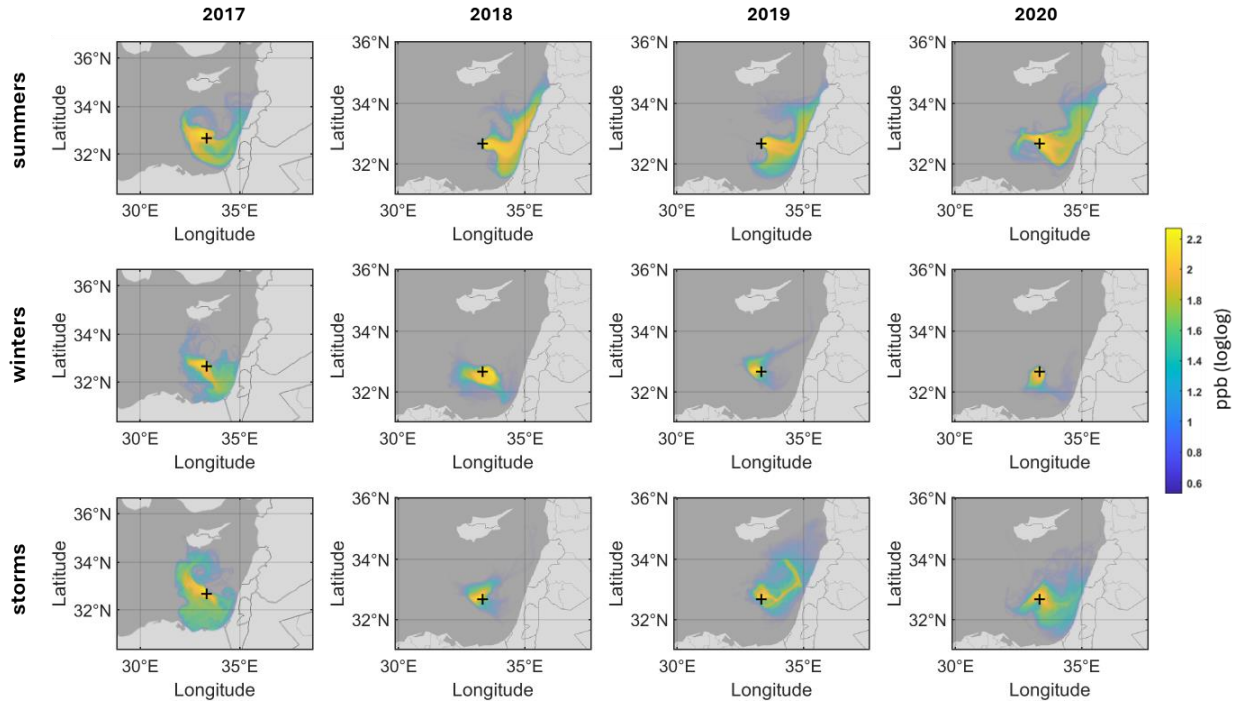

Figure 5 Total hydrocarbon concentration (ppb loglog transformed) in liquid gas phase spills from Block G for the 12 different scenarios. The four panel columns represent the four simulation years 2017-2020 (from left to right).

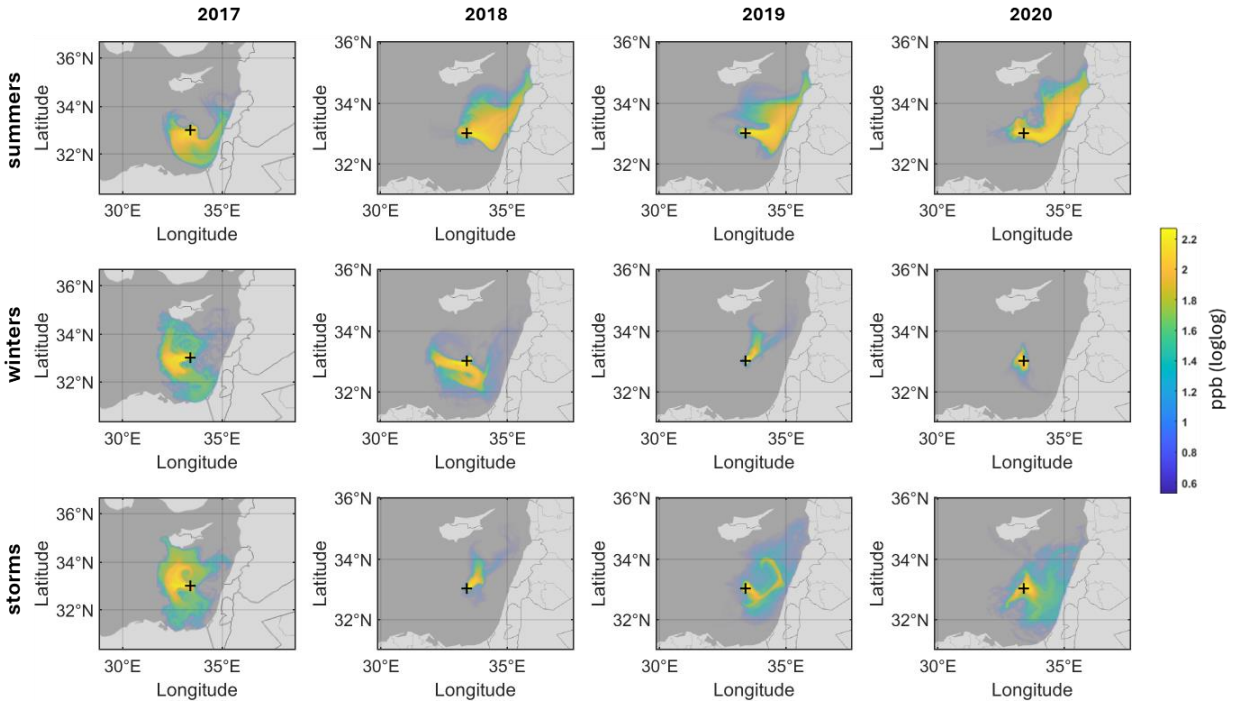

Figure 6 Total hydrocarbon concentration (ppb loglog transformed) in liquid gas phase spills from Block H for the 12 different scenarios. The four panel columns represent the four simulation years 2017-2020 (from left to right).

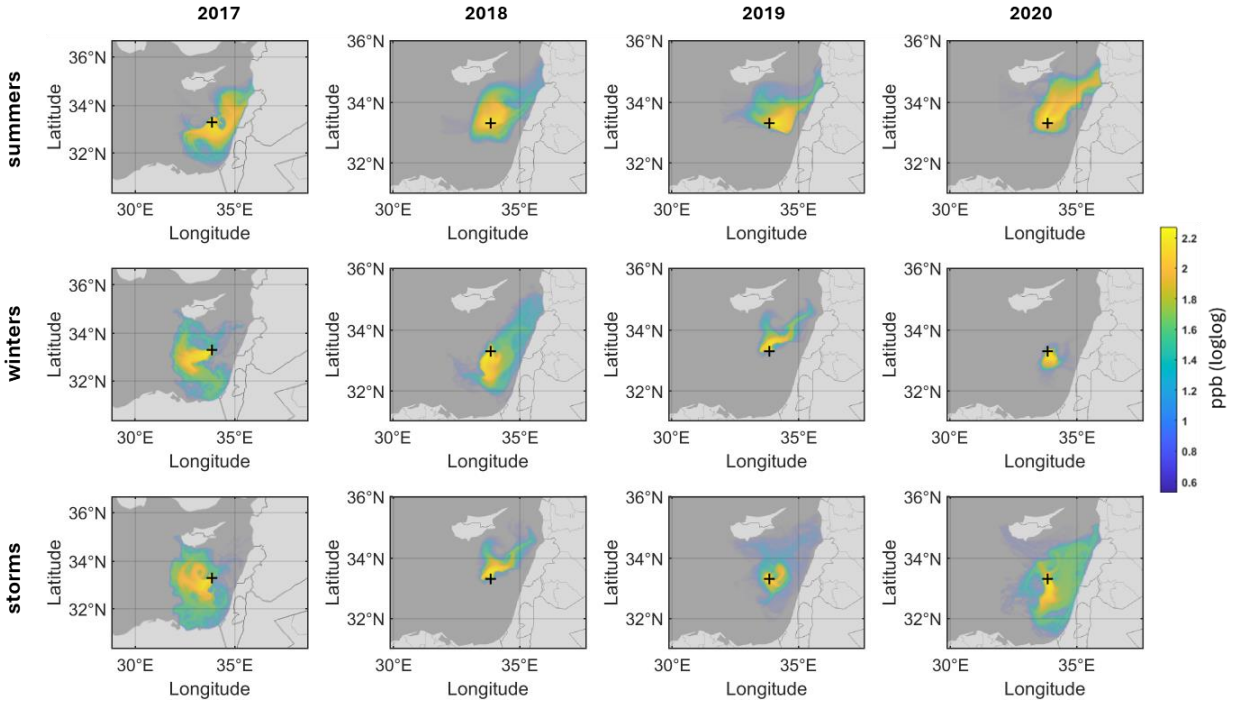

Figure 7 Total hydrocarbon concentration (ppb loglog transformed) in liquid gas phase spills from Block I for the 12 different scenarios. The four panel columns represent the four simulation years 2017-2020 (from left to right).

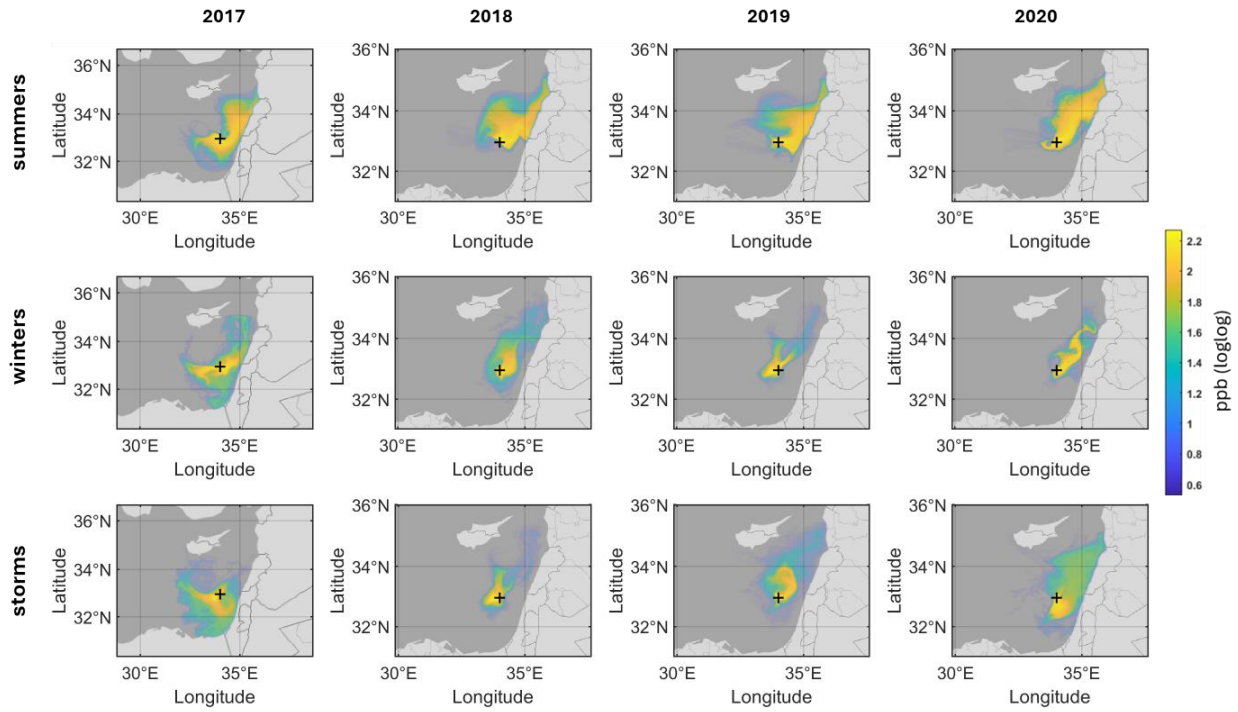

Figure 8 Total hydrocarbon concentration (ppb loglog transformed) in liquid gas phase spills from Tamar for the 12 different scenarios. The four panel columns represent the four simulation years 2017-2020 (from left to right).

Non-Coastal Assets

For non-coastal assets, the primary determinant of impact was the distance from the spill site and a flow towards the north east (Figure 9 and Figure 10). Non-coastal assets showed lower overall exposure compared to coastal assets, with distance serving as a buffer against hydrocarbon pollution. For example, a spill scenario from Block E54 is extends with the currents towards north-east with concentrations diminishing with distance (Figure 9).

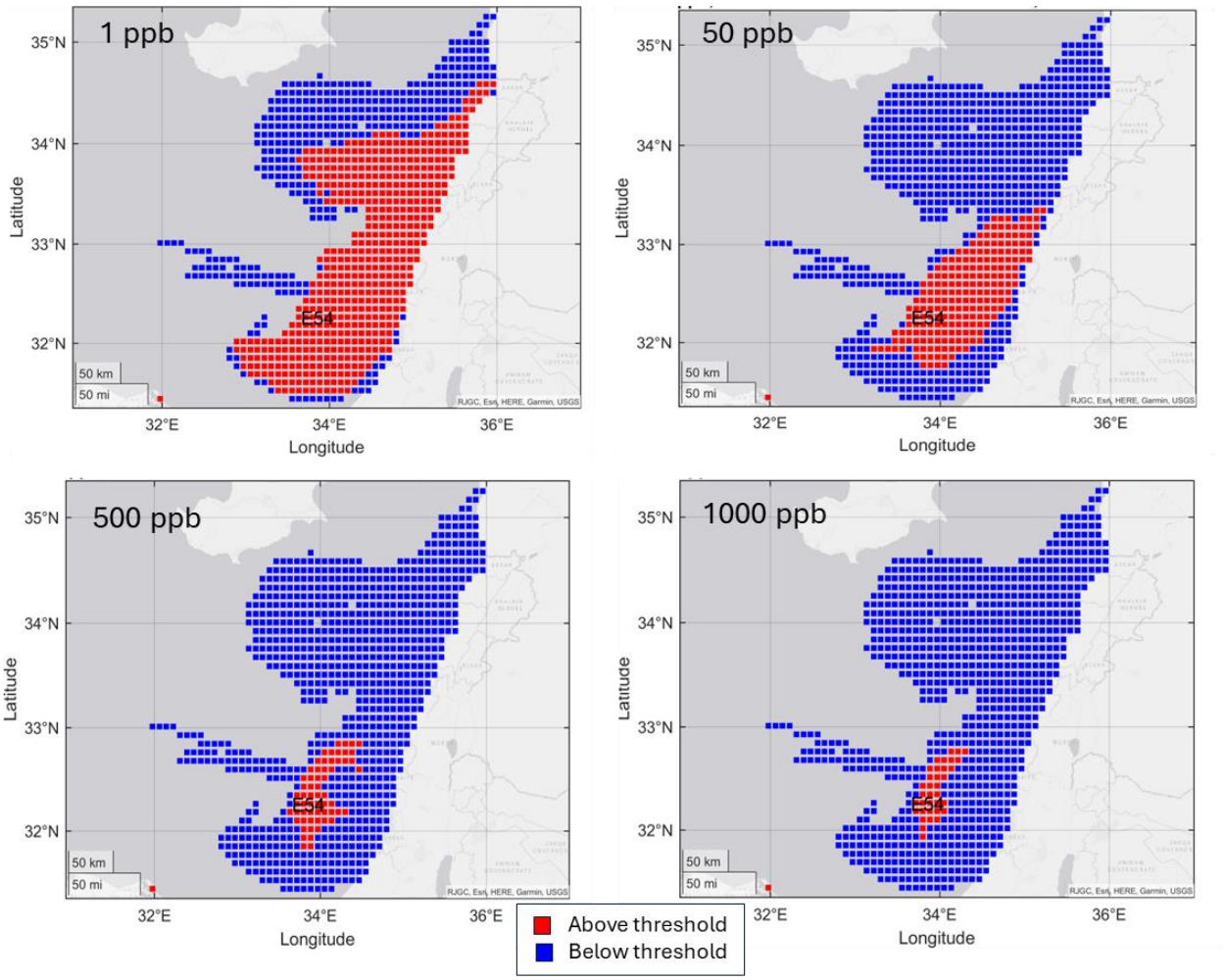

Figure 9 An example of a summer scenario of spill from zone 54 of block E of liquid gas phase (total hydrocarbons) simulated using the currents for summer 2019 (01.07.2019 – 12.08.2019), such that red and blue cells represent hydrocarbons concentration above and below threshold (given at the top left corner of each panel), respectively.

For proposed Deep-Sea MPAs, a clear trend is observed for strong effects towards north-east while the effect diminishes with distance (Figure 10).

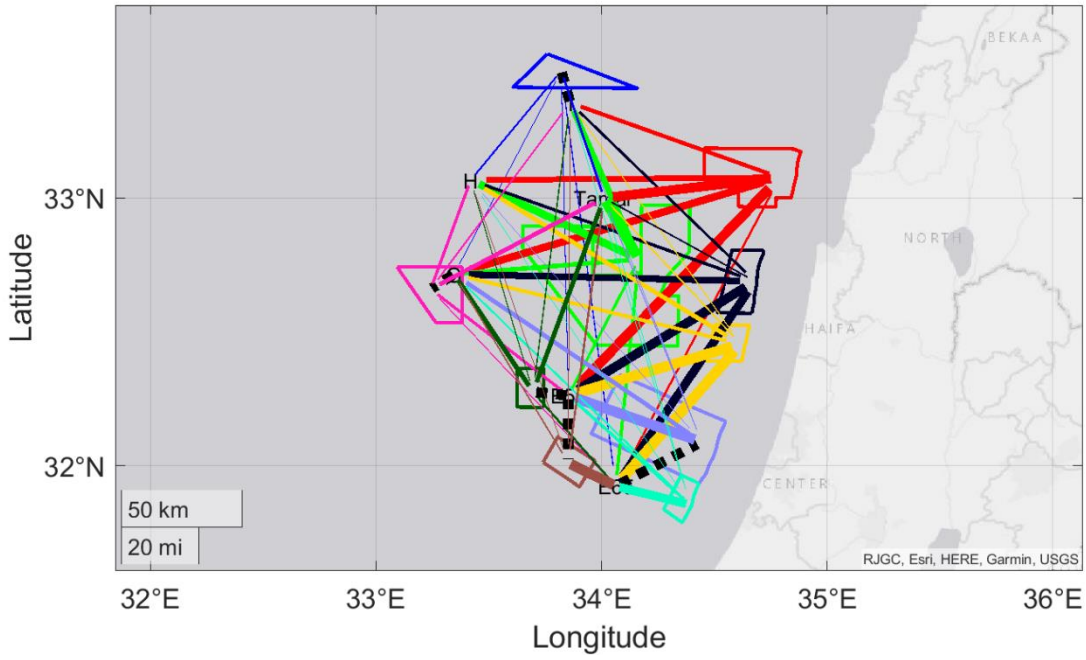

Figure 10 A qualitative comparison of the effects of the different scenarios on the different sites measured in the deep sea MPA's (the max concentration metric. The width of the line is proportional to average effect of all scenarios from a given spills site to a given area. Dashed black lines represent an exceptionally strong effect. Assets: North Levant Channel, Sediment Waves, Heart of the Sea, Dor Slide Base, Patropoda Skeletons, Slope Center, Southern Springs, Palmahim Disturbance, Southern Fan, Southern Slides (see Figure 1 for more details).

Coastal assets - beaches and estuaries as representative cases

All the coastal asset groups showed consistent patterns in the effect of the spill site, latitude and oil type. Here we discuss these general trends using the estuaries and the public beaches for demonstration as they consist of large number of sites that provide a representative gradient.

Effect of Spill Site

Coastal and near-coastal assets were found to be most vulnerable to spills originating from block E, with a particularly high risk from E65, which is situated closer to shore than E54 (e.g., Figure 11). Spills from block G, located further south but still relatively close to the shore, also posed a significant risk. In contrast, spills from blocks H and I, which are further offshore and to the north, exhibited a lower impact (Figure 12, Figure 13). However, assets experienced slightly higher vulnerability to spills from the Tamar site, which is positioned between blocks H and I and closer to shore, particularly during storm events (Figure 13). In addition, a descending north-

south gradient in the severity of the impact is evident when considering coastal assets (Figures 11-19), such that the impact of the spill is higher at the northern areas.

A. Mean

	E54	E65	G	H	I	Tamar
Alexander	7	8.2	3.8	1.9	0.4	0.3
Avtach	3.7	4.2	1.2	1	0.2	0.5
Beit HaEme	8.3	11	6.4	2.5	1.7	2.1
Betzet	8.6	11.2	6.7	3.4	2.2	3.6
Dalia	7.7	10.3	4.3	1.6	0.9	0.5
Gaaton	8.6	11.2	6.5	2.9	1.8	2.6
Hadera	7.2	9.6	3.7	1.6	0.3	0.2
Kishon	7.8	9.9	4.4	1.9	1.1	1.4
Kziv	8.5	11.3	6.5	3	1.8	3.3
Lachish	4.5	4.9	1.4	1	0.4	0.3
Mearot	8.1	11.4	4.6	1.8	1.3	1
Naaman	7.5	9.5	5.9	1.7	1.4	1.7
Oren	8.2	11.7	5.6	2	1.5	1.2
Poleg	5.2	6.1	3.4	1.6	0.5	0.1
Shikma	3.6	4.5	1.3	0.4	0.5	0.5
Sorek	4.7	5.2	2.5	1	0.6	0.2
Taninim	7.8	10.3	4.7	1.7	0.8	0.2
Yarkon	4.8	5.8	2.9	1.6	0.5	0.1
Yasaf	8.2	10.5	6.1	2.5	1.6	1.8

B. Standard deviation

	E54	E65	G	H	I	Tamar
Alexander	6.6	7.9	6	4.5	0.8	0.8
Avtach	5.4	6.5	1.9	2.1	0.6	1.6
Beit HaEme	9.8	10.8	8.3	3.8	3.9	4.2
Betzet	9.6	10.5	8.8	5.4	4.6	5.9
Dalia	7.9	9.4	6.7	3.8	1.9	1.1
Gaaton	10.1	10.6	8.6	4.4	4.1	4.8
Hadera	6.8	8.4	5.2	3.4	0.6	0.6
Kishon	9.7	10.6	5.9	3.8	2.6	2.9
Kziv	9.7	10.7	8.6	5	3.9	5.7
Lachish	5.8	6.5	2.3	2.5	1	1
Mearot	8.8	10.1	5.8	3.9	2.5	2.3
Naaman	9.4	10.4	7.6	2.9	3.1	3.9
Oren	8.9	10.9	6.8	4.1	3	2.6
Poleg	5.5	7.2	5.1	3.8	1.1	0.4
Shikma	6.5	7.1	2.6	1.1	1.5	1.5
Sorek	5.1	7	4.2	3	1.4	0.6
Taninim	8.2	9.1	6.4	3.8	1.5	0.6
Yarkon	5.7	7.9	4.9	3.4	1.2	0.4
Yasaf	9.9	10.6	8	3.7	3.8	3.9

Figure 11 Mean (A) and standard deviation (B) of number of days in which each of the estuaries was exposed to at least 1 ppb. Note the stronger impact of block E.

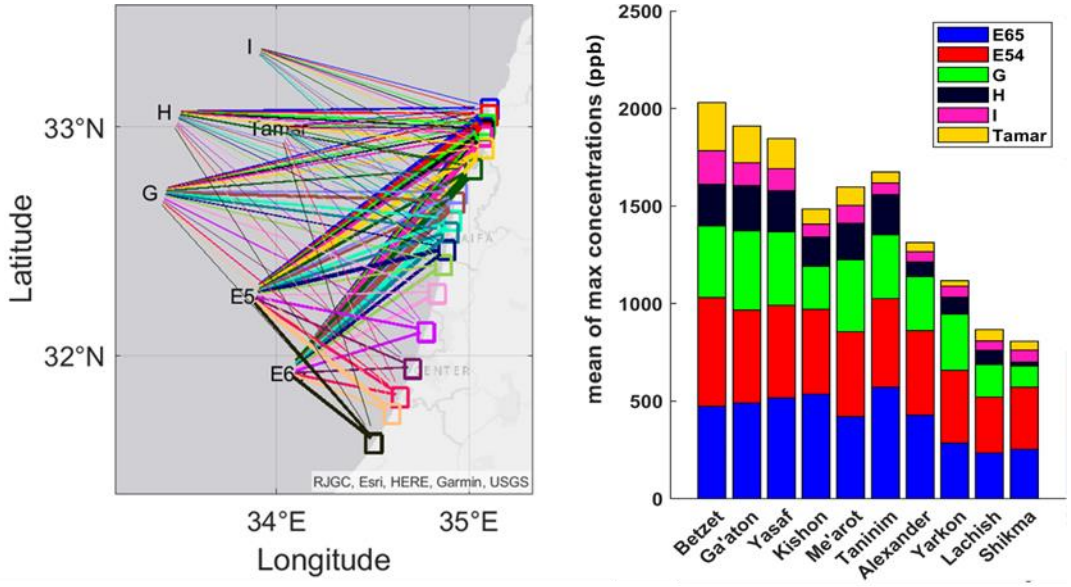

Figure 12 Mean of max concentration per spill site (cumulative) of estuaries shows a clear south-north pattern, while the strongest effect is of spills from block E (blue, red) and to a lesser degree G. The local minima in the northern side stands for the area that are protected by Haifa bay. North to south: Betzet, Kziv, Ga'aton, Beit HaEmek, Yasaf, Na'aman, Kishon, Oren, Me'arot, Dalia, Taninim, Hadera, Alexander, Poleg, Yarkon, Sorek, Lachish, Avtach, Shikma. Note that although summed concentration values are not meaningful on their own (i.e., Betzet beach does not receive maximal concentration of ~1950 ppb, rather it receives separately the mean maximal

amounts from each pollution site), this visualization shows which assets experience the most pollution events with high maximum hydrocarbon concentrations and which pollution sites have a high impact in these cases.

General trends for beaches show coherence in the trends of latitude, spill origin and oil type (Figure 13). Stranded mass along the beaches grouped by the different spill sites, and ordered north to south for each site. We can see higher values from block E, and to some extent G. The northern sites accumulate the scenarios of the strongest effect (the peak at the lefthand side of each spill site). Crude oil (filled markers) gives higher weight than liquid gas phase (empty markers) in consistent similar pattern, while the strongest effects are in the summer (round markers). The north side of spills from blocks H, I , and Tamar also affected in some scenarios, especially in Summer (H,I) and during storm events (Tamar).

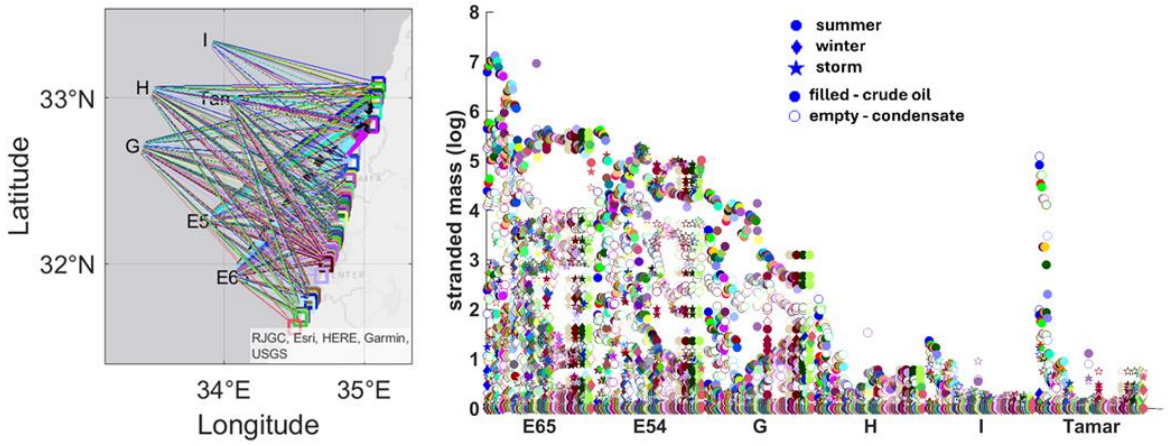

Figure 13 Stranded mass along the beaches grouped by the different spill sites, and ordered north to south for each site. Assets (from south to north): Betzet Beach, Achziv Park Beach, Achziv Beach - Southern Station, Separate Beach Section 1, Separate Beach Section 2, Gali Galil Beach, Sokolov, Shavei Zion Beach, Argaman Beach, Tamarim Beach, Zebulun Beach, Kiryat Haim Beach - Station No. 1, Bat Galim, Kiryat Haim Beach - Station No. 2, Kiryat Haim Beach - Station No. 3, The Quiet Beach, Carmel Beach - Northern Station, Carmel Beach - Southern Station, Dado-Zamir Beach - Station No. 1, Dado-Zamir Beach - Station No. 2, Dado-Zamir Beach - Station No. 3, Dado-Zamir Beach - Station No. 4, Dado-Zamir Beach - Station No. 5, Neve Yam Beach, Dor Beach - Station No. 1, Dor Beach - Station No. 2, Dor Beach - Station No. 3, Jisr, Aqueduct Beach, Caesarea Port, Sea Village, Givat Olga Separate Beach, Givat Olga Central Beach, Givat Olga Southern Beach, Mikhmoret - Station No. 1, Mikhmoret - Station No. 2, Beit Yanai, Neurim Beach, Kiryat Sanz, HaOnot Beach, Amphi Beach, Herzl, Sironit A

Beach, Sirionit B Beach, Argaman Beach, Poleg Beach, Shefayim-Ga'ash, Nof Yam, HaSharon, Zebulun, Arcadia North Beach, Arcadia Center Beach, Arcadia South Beach - Disabled, Separate Beach, Cliff Beach - Station No. 1, Cliff Beach - Station No. 2, Tel Baruch Beach - Station No. 1, Nordau Beach (Metzitzim), Nordau Separate Beach, Hilton North, Gordon, Frishman, Bograshov, Allenby (Jerusalem), Aviv Beach, Charles Clore, Jaffa-Givat Aliya, Jerusalem, HaSela - Station No. 1, HaSela - Station No. 2, HaSela - Station No. 3, Example Beach, The Riviera, Separate Beach, Tayo, Rishon LeZion Beach - Station No. 4, Rishon LeZion Beach - Station No. 3, Rishon LeZion Beach - Station No. 2, Rishon LeZion Beach - Station No. 1, Palmachim Beach, Mei Ami Beach, Lido, Oranim, Arches Beach, Quarter Ya, Riviera, Nitzanim, Bar Kochva, Delilah, Ashkelon National Park Beach, Zikim.

A clear latitudinal gradient was observed in the exposure of coastal and near-coastal assets. Assets along the northern coast experienced greater pollution, with exposure decreasing progressively towards Palmachim. South of Palmachim, there was a slight increase in exposure, primarily due to the high variability of pollution from nearby block E scenarios (Figure 12, Figure 13).

Effect of Oil Type

Heavier oil types consistently produced more extreme values across all metrics, particularly in blocks E and G. Although heavy oil generally exhibited a greater impact, especially in high-risk scenarios, this trend was not entirely deterministic for lower-impact scenarios, where variability was observed (Figure 13).

Detailed results for the different assets groups

In this section, we present a breakdown of the simulation results for each asset group, providing a closer examination of the key trends observed under varying environmental and spill-specific conditions. While mean values and standard deviations are reported for each group as standard statistical measures, it is important to note that these metrics offer limited insight into the complex, non-linear behavior of oil spills. Therefore, the focus here will be on identifying the major patterns and deviations specific to each asset group, as well as discussing the implications of these results in the context of spill response and risk management.

Desalination stations

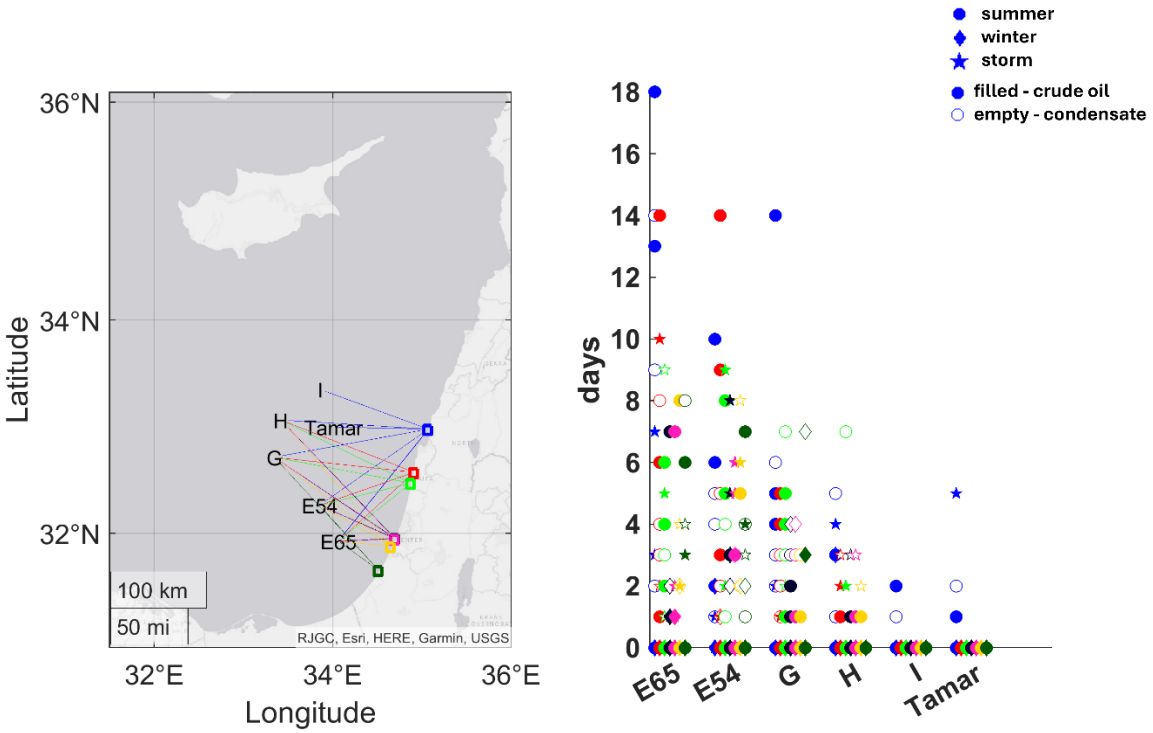

Figure 14 Number of days in which each station was exposed to hydrocarbons concentration of above 500 ppb. The general trend of stronger effect from Block E mainly on the northern sites is preserved. The desalination plants include (from South to North) Ashkelon, Ashdod, Sorek, Palmachim, Hadera, Western Galilee.

The spatial general trends outlined above are applicable to the desalination stations, with the northeastern station being the most exposed. The most significant impact is observed during summer scenarios involving crude oil spills originating from block E, and to a lesser extent, from block G. The Ashkelon station, due to its proximity to block E, specifically region 65, may also be significantly affected by spills, although the likelihood is somewhat lower. In some scenarios, severe exposure levels exceeding 500 ppb (threshold for desalination; Ogunbiyi et al., 2023) are anticipated for over two weeks, and in rare cases, up to three weeks (Figure 14). The maximum hydrocarbon mass that reached the various power plants in the simulated scenarios highlights a pronounced northeastward trend and demonstrates the significant influence of summer spills. Additionally, spills originating from the Tamar area are shown to potentially affect all monitoring stations during storm events (Figure 15).

Power plants and ports

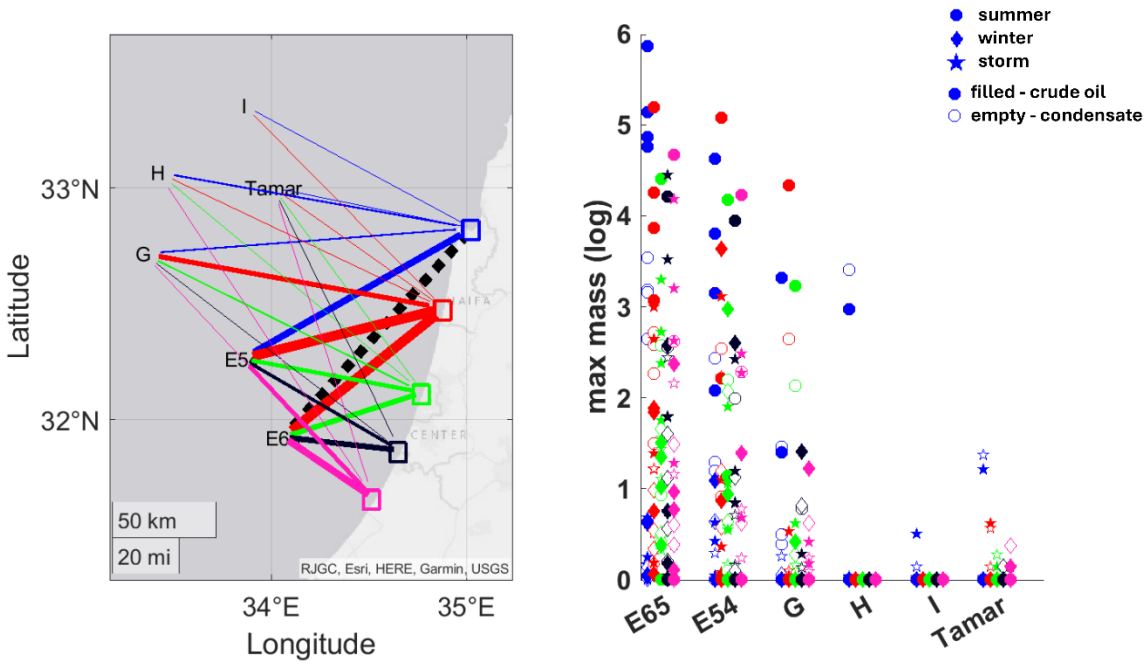

Figure 15 Logarithmic representation of the maximum hydrocarbon mass (kg) that reached the various power plants in the simulated scenarios. The ports depicted are (from south to north) Ashkelon, Ashdod, Tel-Aviv, Hadera, and Haifa.

Similarly to the results of the desalination stations and the spatial general trends outlined above the northern power plants and ports, are the most exposed (Figures 15, 16) . The most significant impact is observed during summer scenarios involving crude oil spills originating from block E, and to a lesser extent, from block G. Spills from Tamar area may impact all stations during storm events.

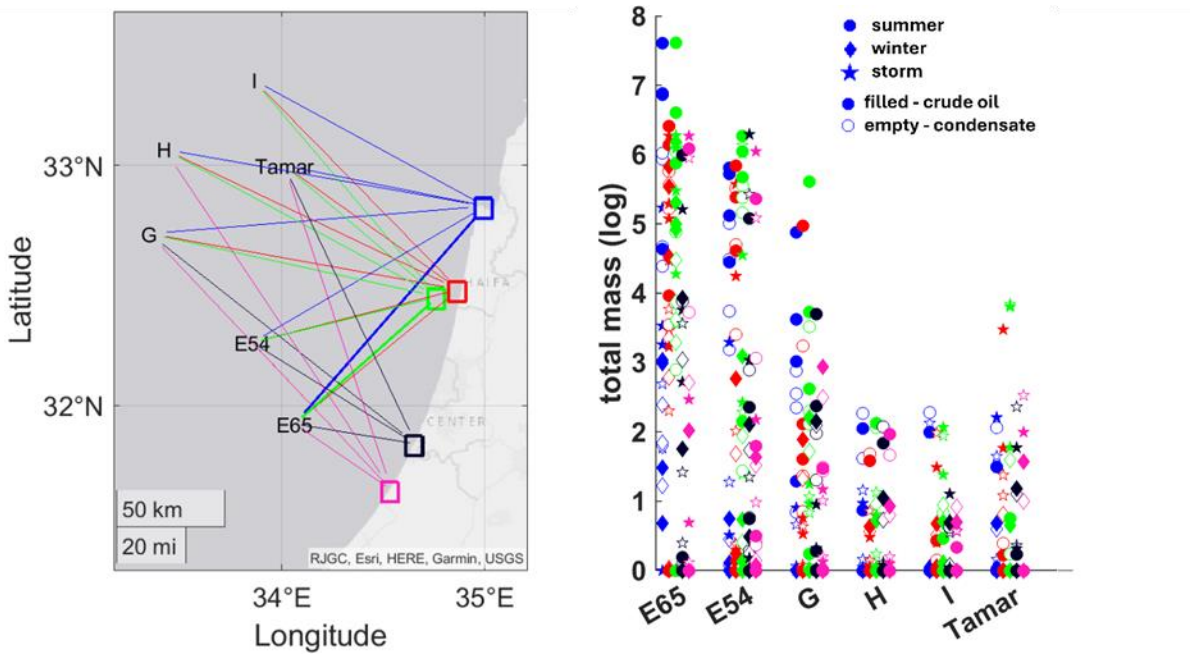

Figure 16 Total mass log (kg) arriving to different ports in the simulated scenarios. The general trends of stronger effect of crude oil during summer towards north-west is preserved. Note that for the total mass the difference between the effects of the different spill sites are less significant than when relating to peaks (e.g. maximal concentration). The ports include (from South to North) Ashdod, Tel-Aviv, Hadera, and Haifa.

Mariculture

Comparable trends have been observed for maricultural areas (Figures 17, 18), although the differential impacts of various spill sites are slightly less pronounced, likely moderated by the distance from the coastline. Nonetheless, significant exposure to PAH exceeding 50 ppb, which is highly toxic, and above the concentration that produce visible slicks (Berenshtein et al., 2020a) is still anticipated, predominantly from block E, and was observed in our scenarios for several days, extending up to four days. Exposure to 1ppb PAH is more common.

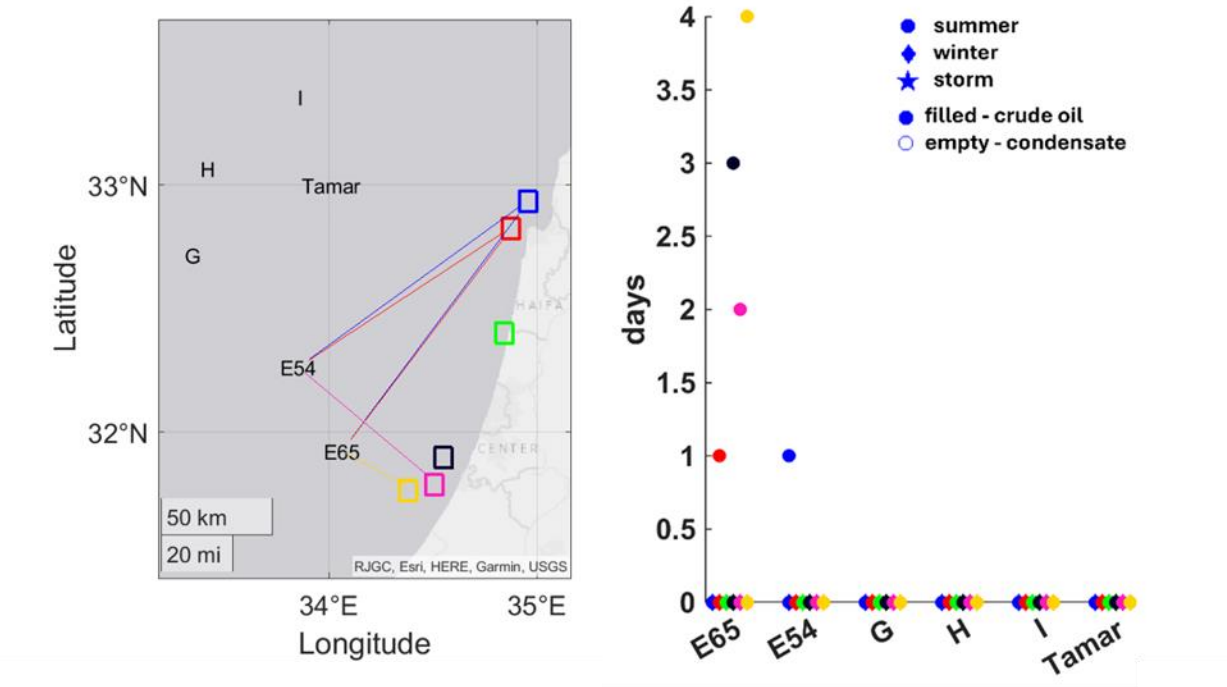

Figure 17 Exposure duration (days) of mariculture areas to at least 50ppb PAH in different maricultural areas. Note the domination of scenarios simulated from block E. The mariculture areas (from South to North) Ashkelon, Ashdod, Tel-Aviv, Hadera, Haifa, and Akko.

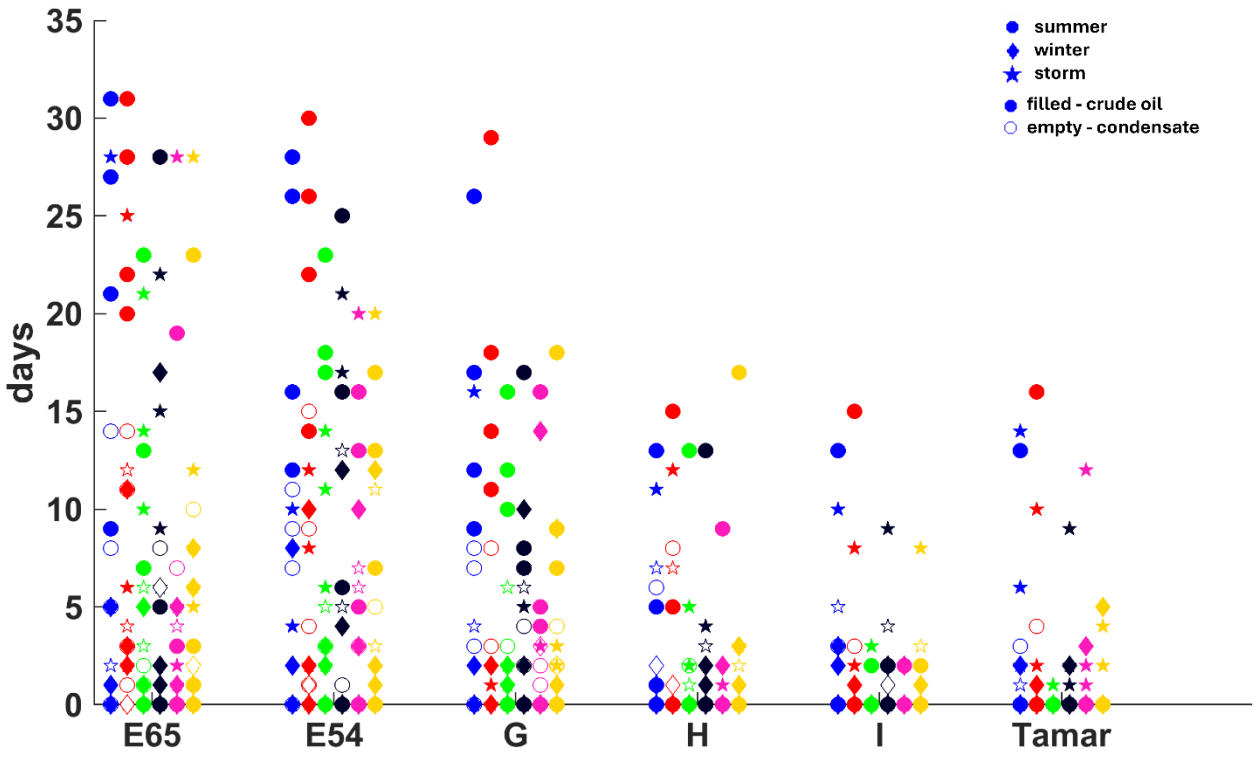

Figure 18 Exposure duration (days) of mariculture areas to at least 1 ppb PAH pollution. This concentration causes significant mortality in the larval stages (Deepwater Horizon Natural Resource Damage Assessment Trustees et al., 2017).

Israel territorial waters MPAs

The potential impact on MPAs, Consistent with the general trends, demonstrating that the most severe impact is attributed to block E, followed by block G, particularly during summer crude oil scenarios affecting northern sites. Spills originating from Tamar may exert an impact during storm events. Similar to the trends observed in maricultural areas, the differences between the effects of different spill sites were less pronounced than those observed in the assets of coastal areas. Block E remains more susceptible to severe impacts on northern sites; however, PAH concentrations of 1 ppb, which can cause significant larval mortality, were observed across all sites (Figure 19). Notably, the deep-sea mesophotic MPAs of Yam-Poleg, Yam-Atlit, and Rosh Karmel are as well mostly affected by blocks E54 and E65, resulting in possible durations of >25 d of toxic-to-marine wildlife concentrations (PAH>1 ppb).

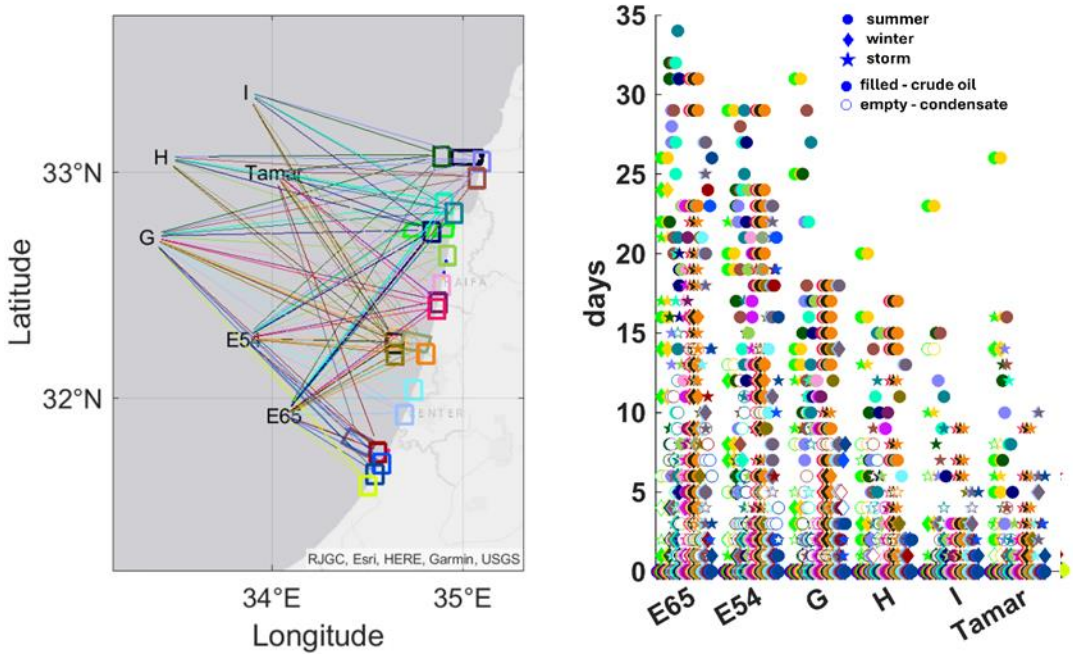

Figure 19 Exposure duration (days) of over 1ppb PAH for the different marine protected areas. Note that such concentration causes a significant mortality for larval and plankton communities. The MPAs (from South to North) Yam Ashqelon, Yamit Evtah Darom, Yam Evtah, Yam Apoloniya, Yafo-Givat Aliya, Yam Palmahim, Yam Shiqma, Yam Poleg, Yam Mikhmoret, Yam Gador, Yam-Qesarya, Yam Dor Ha-Bonim, Yam Atlit - Rekhes Amok, Shiqmona, Yam Rosh Karmel, Yam Shave-Ziyyon, Bustan HaGalil, Yam Rosh Haniqra – Akhziv.

Beaches and estuaries

The extensive number of sites provides a higher resolution perspective, enabling a clearer observation that the summer stranded mass exerts the greatest impact on summer crude oil spills, with a more pronounced effect on northern sites. A similar trend was observed among liquid gas phase scenarios, albeit with a lower stranded mass, as indicated by the empty circles. Tamar exhibited a significant impact during storm events, with the impact strength increasing for sites located along the same latitude.

Discussion

Our analysis revealed a high degree of consistency among the various metrics (total mass, maximum concentration, exposure duration, and stranded mass). These metrics generally reflected the same trends, as described below, indicating that the impact on assets as estimated by the different metrics are correlated, with impact ranked from high to low E > G > H > Tamar > I, which was consistent across coastal and continental shelf assets (MPAs, mariculture, ports, beaches, and estuaries). In addition, the consistency was also evident across the metrices, for example storms from Tamar that result in higher total oil mass will also result in a higher number of days in which concentration is higher than the concentration benchmark threshold. Notably, the variations in total mass arriving at the spill sites are less pronounced than those observed in maximum concentrations, though they follow similar trends across sites. Importantly, a parameter sensitivity test, in which we modified key parameters of hydrocarbon type, turbulence, biodegradation, and input current fields), demonstrated a consistency across the results (Annex 2), further strengthening our conclusions.

Our analysis demonstrated that the location of the spill has tremendous effect on the combined impact of the spill scenario, with the southern regions (block E) being the most impactful. Hence, the choice of drilling areas has a significant impact on the risk to the marine environment and strategic assets along the coast, the continental shelf, and in the open sea, some of which are essential for the economy.

In addition, we find that type of pollutant effects the spill outcome, such that crude oil spills are expected to last longer compared to gas in liquid phase (liquid gas phase-like material). However, from a 2-D spatial perspective, the difference between the two is relatively small (see Annex 3; Figure C1). In contrast, from a vertical perspective, the spatial distribution of hydrocarbons along the water column is different between the two pollutant types due to the difference in hydrocarbon particles' buoyancy (Faillettaz et al., 2021). With respect to our analyses, which examines possible impacts to assets', the difference in the vertical dimension makes a small difference, and the dynamics are governed by the horizontal dynamics, which in turn is dominated by the dynamics at the sea surface (Berenshtein et al., 2020a; Perlin et al., 2020).

We also find a substantial effect of the timing of Spill: inter-annual and inter-seasonal variability in oceanic conditions influence the outcome of the spill, resulting in variability in the hydrocarbon spill extent, and hence its impact. Specifically, spill during the summer months is expected to have the most significant impact on strategic coastal assets (MPAs in territorial waters, desalination facilities, ports, mariculture farms, and beaches) compared to Spill in other seasons. Notably, pollution from the "Tamar" gas field is expected to reach the shore mainly during storm events.

Of all the sites that were recently marketed by the Ministry of Energy for gas explorations, spills from Block E pose the greatest risk to coastal assets, including nature reserves, desalination plants, ports, aquaculture farms, and beaches. Block E spills could lead to significant pollutant levels, potentially shutting down desalination plants for up to 21 days, with the highest risks at northern most desalination site of the western Galilee. Nature reserves and aquaculture farms in the north may face toxic exposure for over two weeks, while protected areas like "Palmachim Slide" in the exclusive economic zone could also be severely affected. The Spill site with the least potential damage is Block I.

Spill risks are particularly significant when spilling from a well in Block E. Spills from blocks in Block E and Block G are expected to cause the highest pollutant mass in desalination plants and could lead to shutdown of desalination facilities for an average of six days, with a maximum shutdown of 30 days, during which pollutant levels would be above the desalination activity shutdown threshold. In most spill scenarios from all sites, the highest pollutant mass is expected at the desalination plants of Western Galilee, Hadera and Haifa.

Spills from sites located in Block E are expected to impact most nature reserves in sovereign waters, causing the highest pollutant mass in all reserves. Reserve areas could be exposed to pollutant concentrations above the toxicity threshold for two weeks or more.
In Haifa and Acre mariculture farms within sovereign waters, the highest pollutant mass is expected in most scenarios, with the most significant impact expected from a Spill from Block E. In some scenarios, exposure to pollutant levels above the toxicity threshold is expected for more than two weeks. Similarly, proposed reserves in the exclusive economic block are expected to be impacted by spills closest to them and south. For instance, a Spill from Block E is expected to cause the highest pollutant mass in the existing protected area "Palmachim Slide."

It is important to note the uncertainties and limitations of our approach. When utilizing oil transport and fate models to assess the potential effects of possible oil and gas spills on the eastern Mediterranean, several limitations and uncertainties must be considered. Firstly, the accuracy of these models is heavily dependent on the quality and resolution of input data, such as oceanographic conditions, weather patterns, and the physical and chemical properties of the oil (Perlin et al., 2020). In addition, the chemical, biological, and physical processes that occur in reality are very complex and occur on multiple media (bottom, water column, sea surface, and air), with complex interactions of the oil with water, gas, and air across multiple stages (Passow and Overton, 2021). As such, while oil transport and fate models are invaluable tools for risk assessment and planning, their predictions should be interpreted with caution, and supplemented with empirical data (e.g., remote sensing) and adaptive management strategies (Lubchenco et al., 2012).

Conclusions

The extensive impacts expected from Spill in Block E, marketed for gas exploration within the fourth tender and not yet granted an exploration license, are part the reasons for avoiding fossil fuel development in this area. All results clearly show that the Spill location significantly affects pollutant dispersion on the seabed and in the water column, impacting the ecosystem and strategic assets in the sea, some of which play an economic role. These results serve as important knowledge for decision-making on the development of the fossil fuel industry in Israel's exclusive economic zone in the Mediterranean, as well as maritime spatial planning (MSP). It is suggested to use spatial analysis for environmental impact assessments and prioritization among different sites in the future.

In case of a spill, toxic pollutant concentrations are expected at tens and hundreds of kilometers from the pollution source. The Ministry of Energy currently defines a minimal 1 km safety distance between the drilling site and sensitive habitats (considering regular drilling operations rather than spill effects). The analysis shows that such distance is grossly insufficient in case of even a small-to-medium Spill, hence significantly increasing the safety distance between drilling and sensitive habitats is necessary.

The relative ranking of spill sites by their impact on all assets: Spill from sites in Block E, specifically Block 65, is expected to have the most significant impact on strategic coastal assets -

nature reserves in sovereign waters, desalination facilities, ports, mariculture farms, and beaches. Spilling from Block I will likely have the least impact on all assets.

From a broader perspective, our findings highlight the importance of considering a comprehensive range of natural and socioeconomic assets when evaluating the potential effects of hydrocarbon pollution. It is advisable to use explicit benchmarks to assess the impact accurately. Key metrics might include the extent of areas exposed to concentrations toxic to marine life and the number of days desalination plants may be non-operational. Incorporating such clear and quantifiable benchmarks allows for a more detailed understanding of the ramifications, aiding in effective decision-making and policy development to mitigate risks associated with hydrocarbon pollution.

Acknowledgements

We thank the members of the steering committee, and the researchers that provided valuable comments which substantially improved this report: Dr. Aviv Solodoch, Mr. Ilan Nissim, and IOLR researchers. We also thank Mr. Omri Lapidot for the valuable help with constructing the user interface.

References

Alloy, M., Garner, T. R., Bridges, K., Mansfield, C., Carney, M., Forth, H., et al. (2017). Co-exposure to sunlight enhances the toxicity of naturally weathered Deepwater Horizon oil to early lifestage red drum (Sciaenops ocellatus) and speckled seatrout (Cynoscion nebulosus). *Environ Toxicol Chem* 36, 780–785.

Barron, M. G. (2012). Ecological impacts of the Deepwater Horizon oil spill: implications for immunotoxicity. *Toxicol Pathol* 40, 315–320.

Ben-Ezra, T., Blachinsky, A., Gozali, S., Tsemel, A., Fadida, Y., Tchernov, D., et al. (2024). Interannual changes in nutrient and phytoplankton dynamics in the Eastern Mediterranean Sea (EMS) predict the consequences of climate change; results from the Sdot-Yam Time-series station 2018-2022. *bioRxiv*. doi: 10.1101/2024.06.24.600321

Berenshtein, I., Paris, C., Perlin, N., Alloy, M., Joye, S., and Murawski, S. (2020a). Invisible oil beyond the Deepwater Horizon satellite footprint. *Sci Adv* 6, 8863.

Berenshtein, I., Perlin, N., Ainsworth, C. H., Ortega-Ortiz, J. G., Vaz, A. C., and Paris, C. B. (2020b). "Comparison of the Spatial Extent, Impacts to Shorelines, and Ecosystem and Four-Dimensional Characteristics of Simulated Oil Spills," in *Scenarios and Responses to Future Deep Oil Spills*, (Springer), 340–354.

Berenshtein, I., Stern, N., Tagar, A., Paris, C. B., Lapidot, O., Morov, A. R., et al. (2024). Proposed network of Marine Protected Areas supports larval dispersal and connectivity in the Eastern Mediterranean. *bioRxiv*, 2024.04.28.591505. doi: 10.1101/2024.04.28.591505

Blumberg, A. F., and Mellor, G. L. (1987). A description of a three-dimensional coastal ocean circulation model. *Three-dimensional coastal ocean models* 4, 1–16.

Brenner, S. (2015). Oil spill modeling in the southeastern Mediterranean Sea in support of accelerated offshore oil and gas exploration. *Ocean Dyn* 65, 1685–1697. doi: 10.1007/s10236-015-0902-2

Clementi, E., Pistoia, J., Escudier, R., Delrosso, D., Drudi, M., Grandi, A., et al. (2016). Mediterranean Sea Analysis and Forecast (CMEMS MED. *Currents* 2019.

Cordes, E. E., Jones, D. O. B., Schlacher, T. A., Amon, D. J., Bernardino, A. F., Brooke, S., et al. (2016). Environmental impacts of the deep-water oil and gas industry: a review to guide management strategies. *Front Environ Sci* 4, 58.

Danovaro, R., Company, J. B., Corinaldesi, C., D'Onghia, G., Galil, B., Gambi, C., et al. (2010). Deep-Sea Biodiversity in the Mediterranean Sea: The Known, the Unknown, and the Unknowable. *PLoS One* 5. doi: 10.1371/journal.pone.0011832

Deepwater Horizon Natural Resource Damage Assessment Trustees, Assessment, D. H. N. R. D., and Trustees, D. H. N. R. D. A. (2017). Deepwater Horizon oil spill: Final Programmatic Damage Assessment and Restoration Plan and Final Programmatic Environmental Impact Statement. Available at: http://www.gulfspillrestoration.noaa.gov/sites/default/files/wp-content/uploads/Draft_ERP-PEIS_Part_2_Chapter_4_through_Chapter_9.pdf (Accessed March 21, 2018).

Escudier, R., Clementi, E., Omar, M., Cipollone, A., Pistoia, J., Aydogdu, A., et al. (2020). Mediterranean Sea Physical reanalysis (CMEMS MED-currents)(version 1)[Data set]. *Copernicus Monitoring Environment Marine Service (CMEMS)*.

Faillettaz, R., Paris, C. B., Vaz, A. C., Perlin, N., Aman, Z. M., Schlüter, M., et al. (2021). The choice of droplet size probability distribution function for oil spill modeling is not trivial. *Mar Pollut Bull* 163, 111920.

Geo-prospect Ltd. (2016). Offshore Oil and Gas Exploration and Production Strategic Environmental Assessment (SEA).

Goldman, R., Biton, E., Brokovich, E., Kark, S., and Levin, N. (2015). Oil spill contamination probability in the southeastern Levantine basin. *Mar Pollut Bull* 91, 347–356. doi: 10.1016/J.MARPOLBUL.2014.10.050

Karcz, K., Gellman, Y., Shitrit, O., and Steinberg, J. (2019). The Leviathan Field - Nine Years Since Discovery and Nearing First Gas. *Second EAGE Eastern Mediterranean Workshop*. doi: 10.3997/2214-4609.201903152

Khosla, I. (2020). Israel's Mediterranean Gas: Domestic Governance, Economic Impact, and Strategic Implications. *Strategic Analysis* 44, 279–281. doi: 10.1080/09700161.2020.1784682

Lubchenco, J., McNutt, M. K., Dreyfus, G., Murawski, S. A., Kennedy, D. M., Anastas, P. T., et al. (2012). Science in support of the Deepwater Horizon response. *Proc Natl Acad Sci U S A* 109, 20212–21. doi: 10.1073/pnas.1204729109

Morato, T., Hoyle, S., Allain, V., and Nicol, S. (2010). Seamounts are hotspots of pelagic biodiversity in the open ocean. *Proceedings of the National Academy of Sciences* 107, 9707-9711-9707–9711. doi: 10.1073/pnas.0910290107

Morato, T., Kvile, K., Taranto, G. H., Tempera, F., Narayanaswamy, B., Hebbeln, D., et al. (2012). Seamount physiography and biology in the north-east Atlantic and Mediterranean Sea. *Biogeosciences* 10, 3039-3054-3039–3054. doi: 10.5194/BG-10-3039-2013

Nardelli, B. B., Fratianni, C., Roquet, H., and Santoleri, R. (2004). Regional SST product development and assimilation within the Mediterranean forecasting system.

Needham, D. L., Pettingill, H. S., and Christensen, C. J. (2017). The Tamar giant gas field: Opening the subsalt Miocene gas play in the Levant Basin.

Nelson, J. R. R., Grubesic, T. H. H., Sim, L., Rose, K., and Graham, J. (2015). Approach for assessing coastal vulnerability to oil spills for prevention and readiness using GIS and the Blowout and Spill Occurrence Model. *Ocean Coast Manag* 112, 1–11. doi: 10.1016/J.OCECOAMAN.2015.04.014

Nichols, J., and Parker, H. (1989). EFFECTS OF OIL POLLUTION ON INDUSTRIAL WATER INTAKES1. 1989, 473–478. doi: 10.7901/2169-3358-1989-1-473

Ogunbiyi, O., Al-Rewaily, R., Saththasivam, J., Lawler, J., and Liu, Z. (2023). Oil spill management to prevent desalination plant shutdown from the perspectives of offshore cleanup, seawater intake and onshore pretreatment. *Desalination* 564, 116780.

Ozer, T., Gertman, I., Gildor, H., and Herut, B. (2022a). Thermohaline Temporal Variability of the SE Mediterranean Coastal Waters (Israel) – Long-Term Trends, Seasonality, and Connectivity. 8. doi: 10.3389/fmars.2021.799457

Ozer, T., Rahav, E., Gertman, I., Sisma-Ventura, G., Silverman, J., and Herut, B. (2022b). Relationship between thermohaline and biochemical patterns in the levantine upper and intermediate water masses, Southeastern Mediterranean Sea (2013–2021). 9. doi: 10.3389/fmars.2022.958924

Palumbi, S. R. (2001). The ecology of marine protected areas. *Marine community ecology* 9, 509–530.

Paris, C. B., Hénaff, M. Le, Aman, Z. M., Subramaniam, A., Helgers, J., Wang, D. P., et al. (2012). Evolution of the Macondo well blowout: Simulating the effects of the circulation and synthetic dispersants on the subsea oil transport. *Environ Sci Technol* 46, 13293–13302. doi: 10.1021/es303197h

Passow, U., and Overton, E. B. (2021). The complexity of spills: the fate of the Deepwater Horizon oil. *Ann Rev Mar Sci* 13, 109–136.

Perlin, N., Paris, C. B., Berenshtein, I., Vaz, A. C., Faillettaz, R., Aman, Z. M., et al. (2020). "Far-field modeling of a seep-sea blowout: Sensitivity studies of initial conditions, biodegradation, sedimentation, and subsurface dispersant injection on surface slicks and oil plume concentrations," in *Deep Oil Spills*, (Springer), 170–192.

Sala, E., and Giakoumi, S. (2018). No-take marine reserves are the most effective protected areas in the ocean. *ICES Journal of Marine Science* 75, 1166–1168.

Solo-Gabriele, H. M., Fiddaman, T., Mauritzen, C., Ainsworth, C., Abramson, D. M., Berenshtein, I., et al. (2021). Towards integrated modeling of the long-term impacts of oil spills. *Mar Policy* 131, 104554.

Spanier, E., and Zviely, D. (2022). Key Environmental Impacts along the Mediterranean Coast of Israel in the Last 100 Years. *J Mar Sci Eng*. doi: 10.3390/jmse11010002

Tom, M., and Galil, B. (1991). The Macrobenthic Associations of Haifa Bay, Mediterranean Coast of Israel. *Marine Ecology* 12, 75-86-75–86. doi: 10.1111/J.1439-0485.1991.TB00085.X

Wade, T. L., Sericano, J. L., Sweet, S. T., Knap, A. H., and Guinasso, N. L. (2016). Spatial and temporal distribution of water column total polycyclic aromatic hydrocarbons (PAH) and total petroleum

hydrocarbons (TPH) from the Deepwater Horizon (Macondo) incident. *Mar Pollut Bull* 103, 286–293. doi: 10.1016/j.marpolbul.2015.12.002

Zafirakou-Koulouris, A., Koutitas, C., Sofianos, S., Mantziafou, A., Tzali, M., and Dermissi, S. C. (2012). Oil spill dispersion forecasting with the aid of a 3D simulation model. *Journal of Physical Science and Application* 2.

Annex 1 – SELIPS validation (carried out by Dr. Eli Biton and Yaakov Zaken (IOLR): supplementary section 1 from (Berensnshtein et al. 2024)

In order to examine the performance of the SELIPS model, SELIPS results were compared with measurements in the coastal environment, and in the open sea. These included currents, temperature and (salinity data obtained from the following sources: 1 Two coastal measurement stations located at the ends of the coal piers of the Orot Rabin and Rotenberg power plants in Hadera and Ashkelon, which are (about 2.2 km from the coastline and at a depth of 26 m; 2 The DEEPLEV (mooring) sampling station is located about 45 km northwest of the Haifa coast and at a depth of about 1600 m.

Comparison With stations in Hadera and Ashkelon

Overall, the SELIPS results and the temperature and salinity values measured at the measurement stations in Ashkelon (Lon 34.49917, Lat 31.63472) and Hadera (Lon 34.863070, Lat 32.470530) (Figures A1-4) are well matched as computed using root-mean-square error (RSME). The results of the model closely followed the seasonal dynamics of temperature and salinity. However, in the case of the salinity values, the observed seasonal amplitude is greater and indicates values higher in summer and lower in winter than those obtained based on the results of the model. A possible explanation for these discrepancies is related to factors that are not included. The model runs include the contribution of increased sedimentation of the streams during the winter, particularly during winter storms accompanied by heavy rainfall, and on the other hand, a possible contribution of brine flow from the desalination plants adjacent to the measuring stations. The comparisons between the streams measured in Ashkelon and Hadera and the results of the model are provided in Figures A5-8 and 6-10, respectively. In all cases, the flow observations were taken from a depth of 5 meters, and were taken every three hours to match the model's output. Both the observations of the currents in Ashkelon and Hadera and the results of the model indicate that the coastal flow moves mainly along the coastline, with a clear predominance towards the north. Overall, the results of the model follow the data measured in Hadera nicely (the Fourier norm stands at 0.78), but there is a slight shift of about 10 degrees compared to the data, which apparently originated from the bias of the model and the direction of its coastline compared to the direction of isobaths adjacent to the measuring stations. At the Ashkelon station, it can also be seen that the model tracks seasonal changes in the intensity of the coastal flow, but a less favorable comparison is obtained with the measurements (the Fourier norm is 1.22).

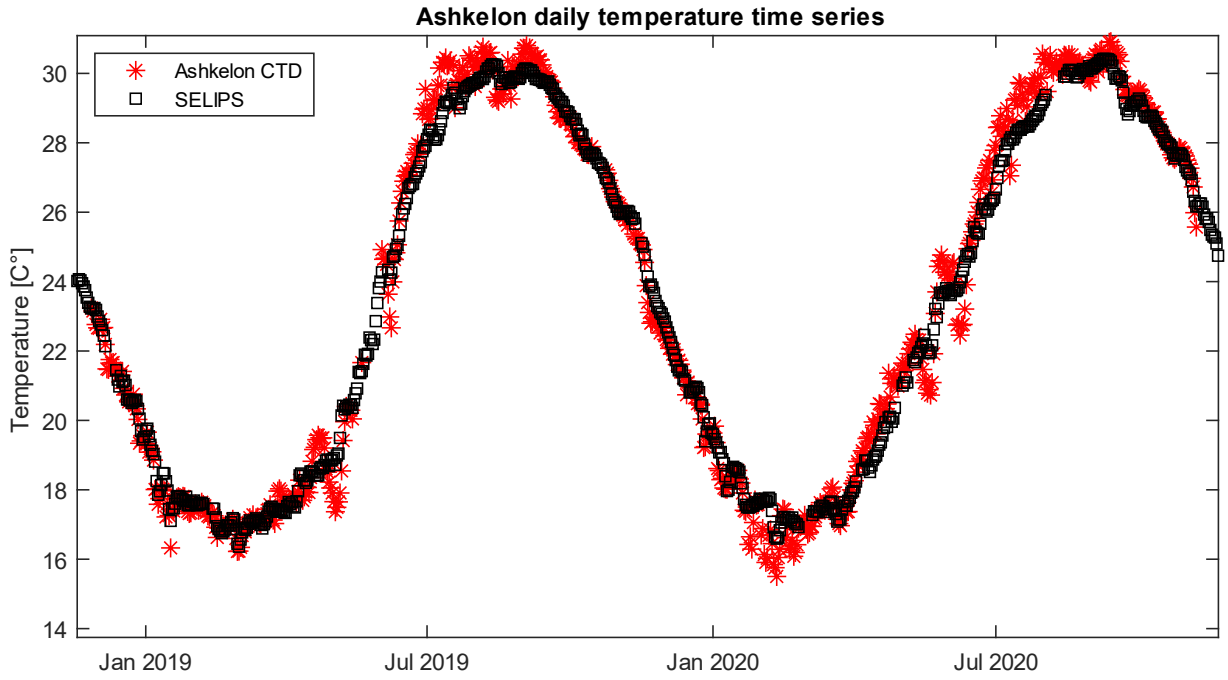

Figure A1. Circadian averages of temperature as measured at the Ashkelon measuring station at a water depth of 11 m (red) against the results of the SELIPS model in the same location. The calculated correlation coefficient between the two time series is 0.99 with an RMSE of 0.55 degrees.

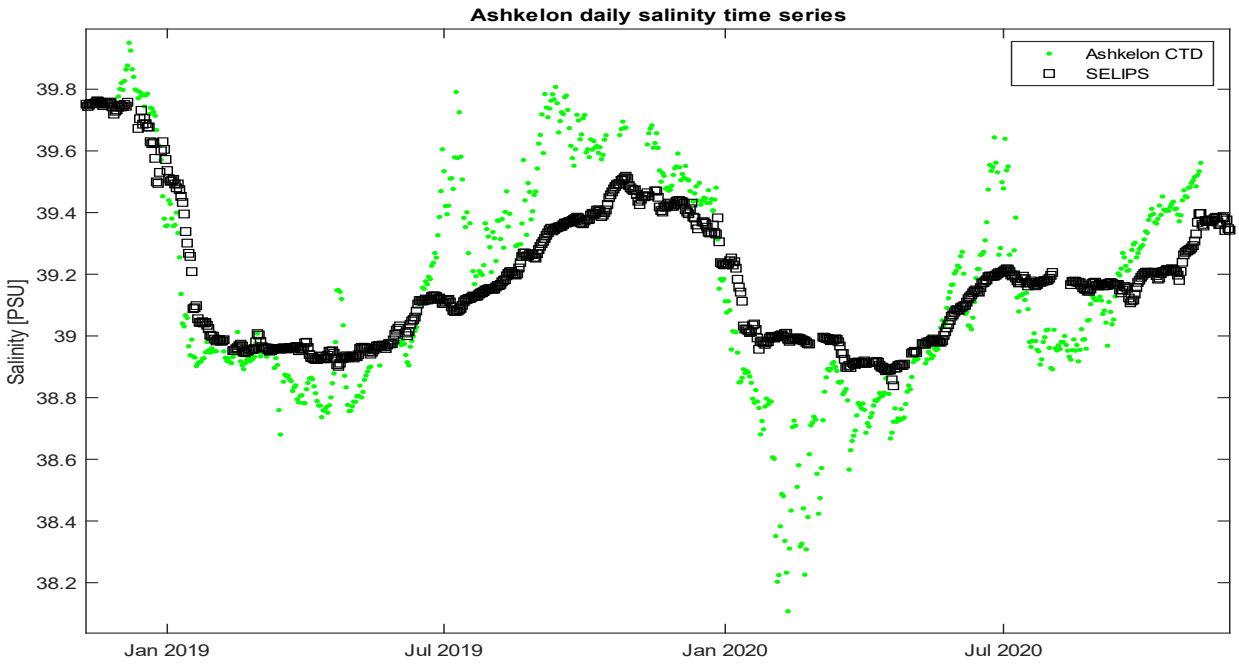

Figure A2. Circadian averages of salinity as measured at the Ashkelon measuring station at a water depth of 11 m (green) against the results of the SELIPS model in the same location. The calculated correlation coefficient between the two-time series is 0.81 with RMSE of 0.2 PSU.

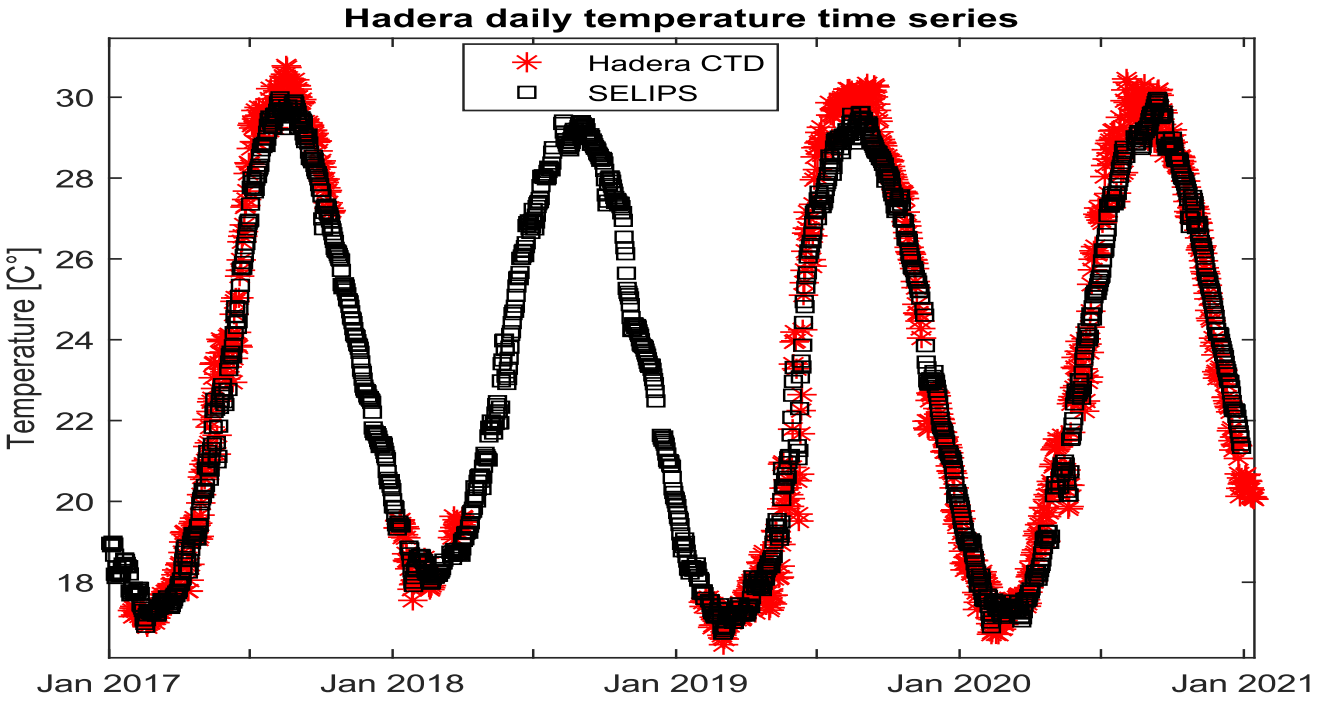

Figure A3. Circadian averages of temperature as measured at the Hadera measuring station at a water depth of 11 m (red) against the results of the SELIPS model in the same location. The calculated correlation coefficient between the two time series is 0.99 with an RMSE of 0.59 degrees.

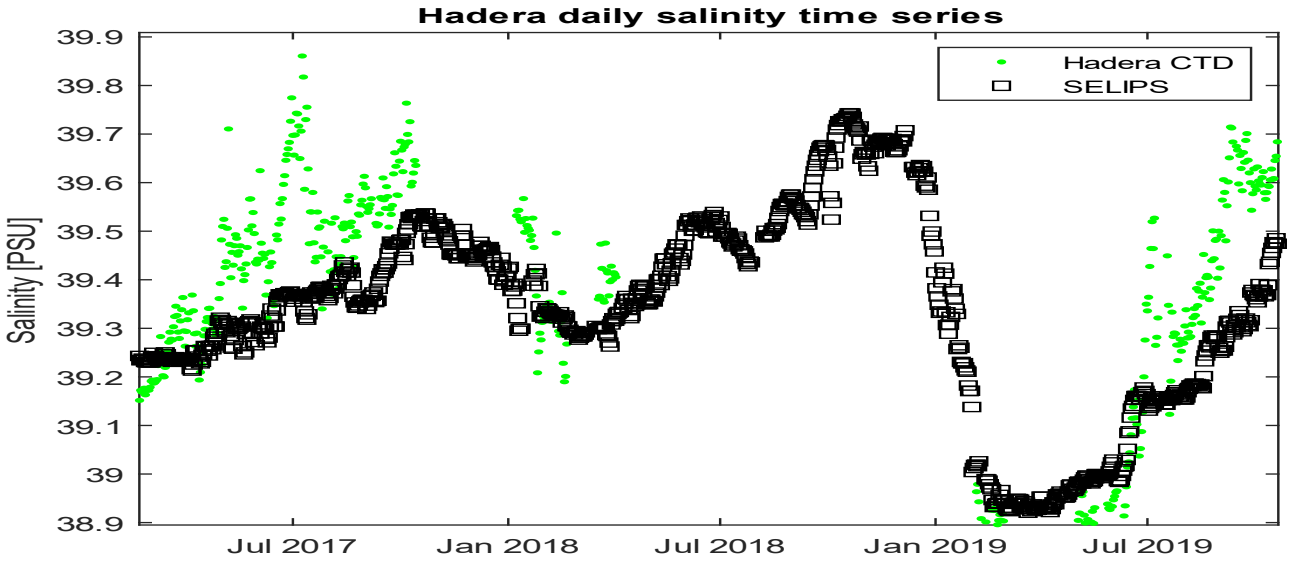

Figure A4. Circadian averages of salinity as measured at the Hadera measuring station at a water depth of 11 m (red) against the results of the SELIPS model in the same location. The calculated correlation coefficient between the two time series is 0. 91 with RMSE of 0.11 PSU.

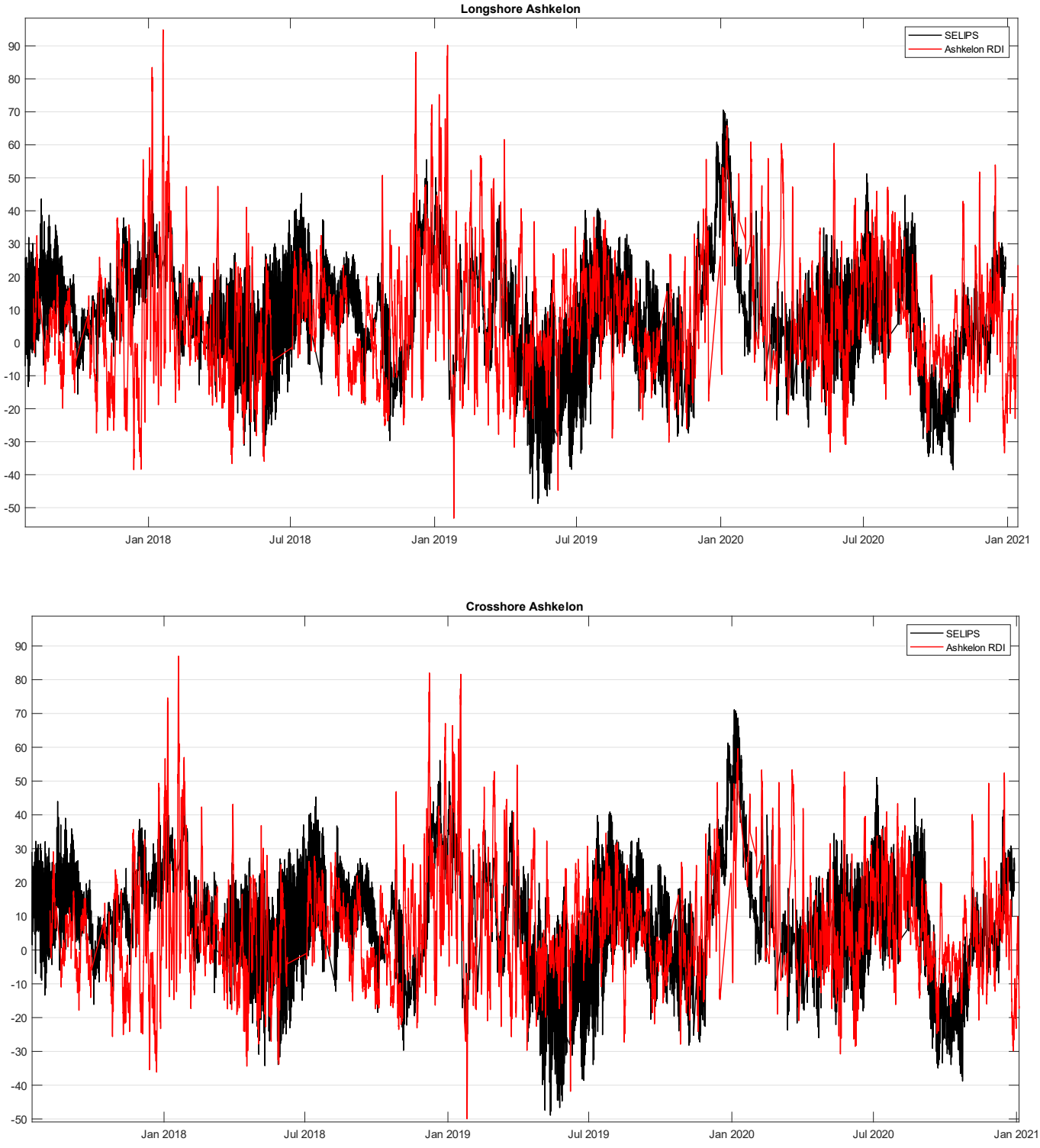

Figure A5. 3-hour averages of the components of the currents along (top) and perpendicular (bottom) to the lines with a depth value as measured at the Ashkelon station between 2021 and 207 at a water depth of 11 m (red) against the results of the SELIPS model in the same position (black). The calculated correlation coefficients between the two time series are 0.37 for the tangential component and 0.34 for the component perpendicular to the isobath.

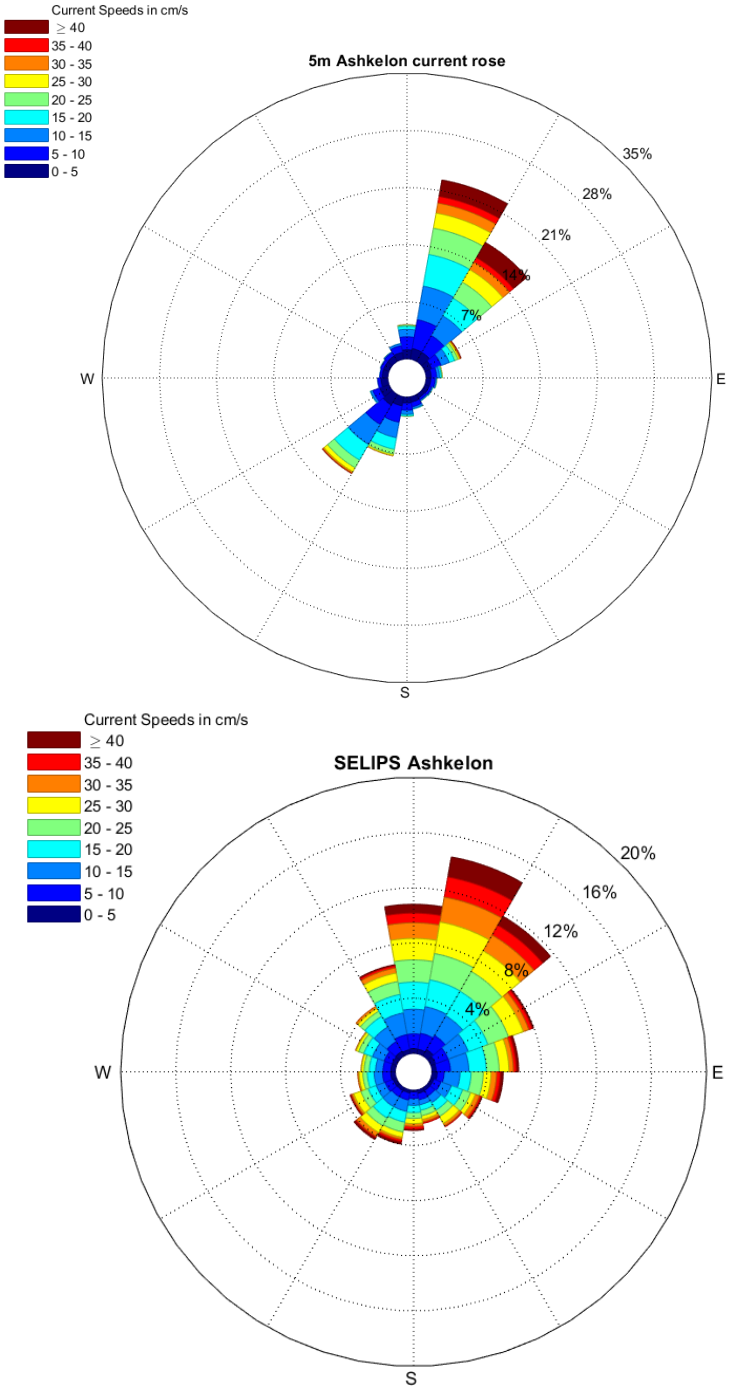

Figure A6. Rose diagram as calculated based on the measurements in Ashkelon at a depth of 5 m (top) for the years 2017-2021 against the results of the SELIPS model in the same location (bottom).

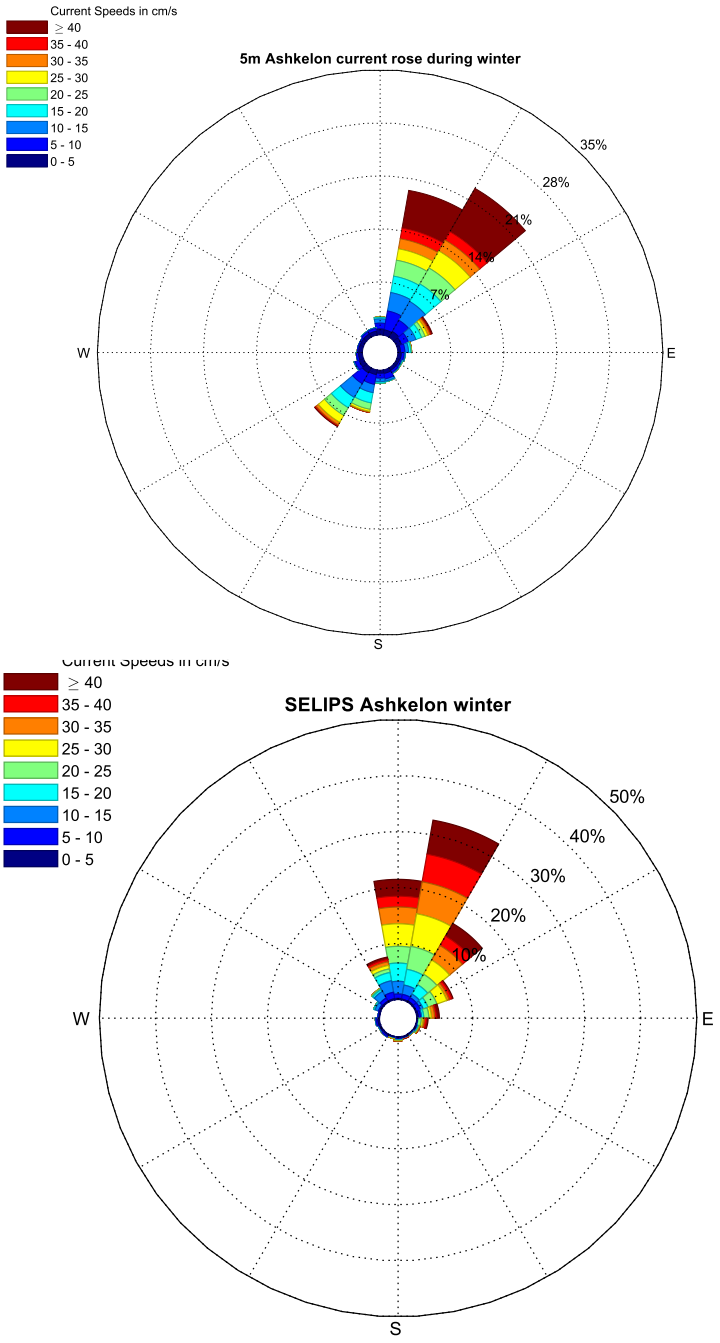

Figure A7. Rose diagram as calculated based on the measurements in Ashkelon at a depth of 5 m (top) in the winters of 2017-2021 against the results of the SELIPS model in the same location (bottom).

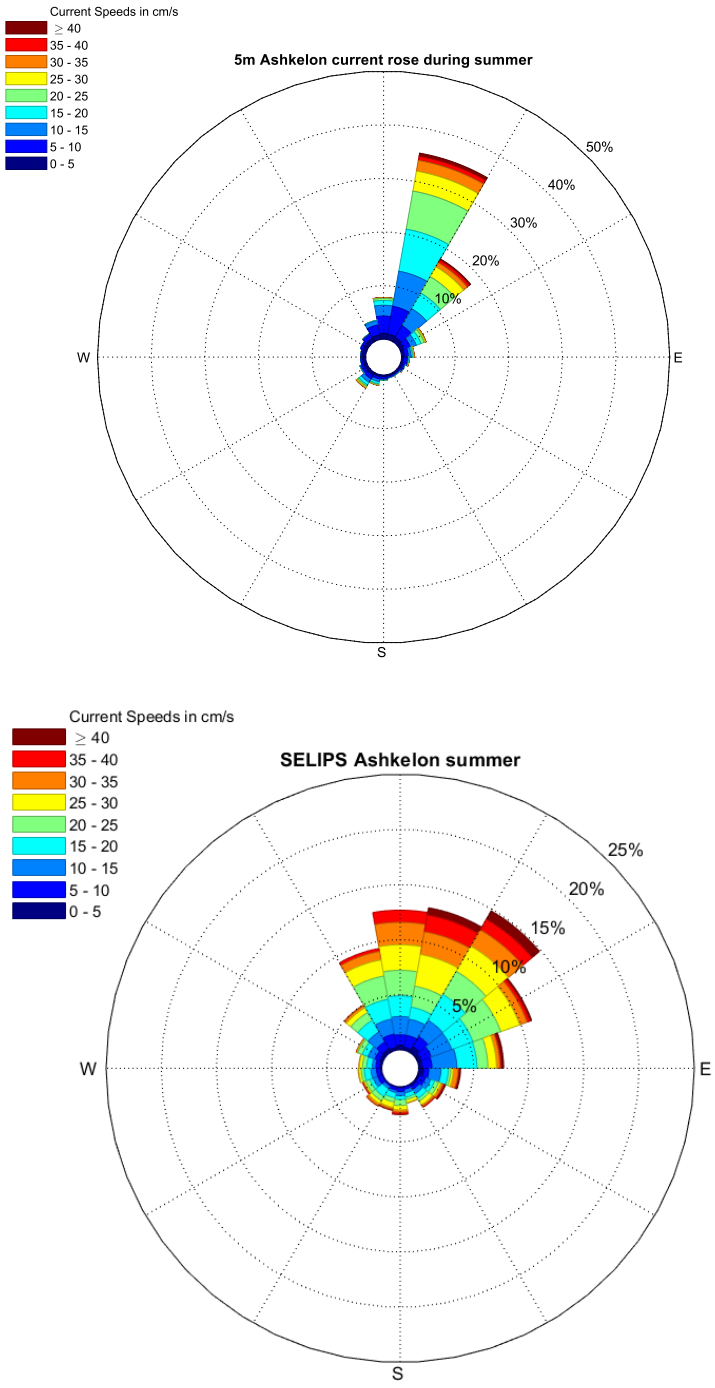

Figure A8. Rose diagram as calculated based on the measurements in Ashkelon at a depth of 5 m (top) in the summers of 2017-2021 against the results of the SELIPS model in the same location (bottom).

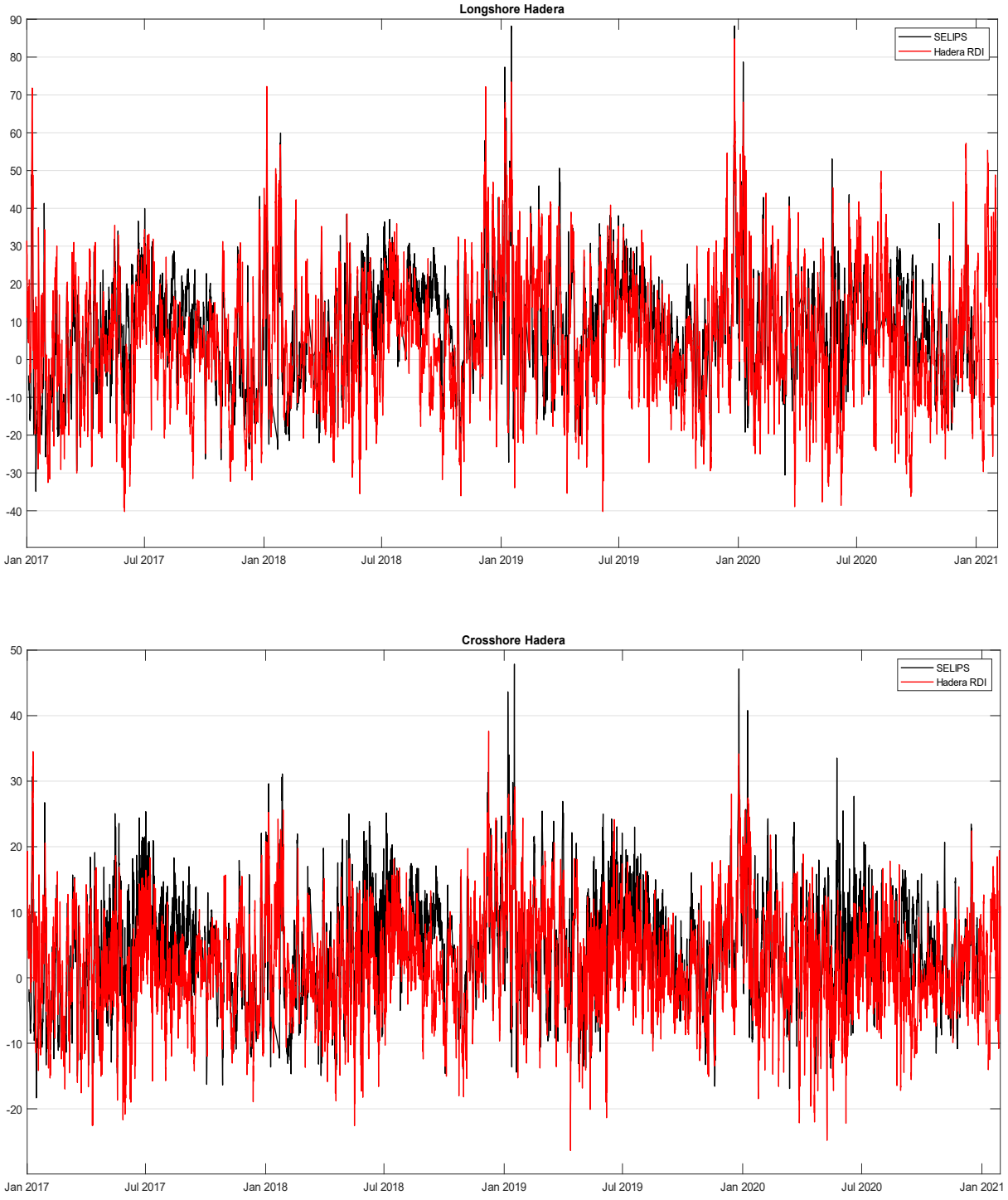

Figure A9. Three-hour averages of the components of the currents along (top) and perpendicular (bottom) to the isobaths as measured at the Hadera station between 2021 and 207 at a water depth of 11 m (red) against the results of the SELIPS model in the same position (black). The calculated correlation coefficients between the two time series are 0.67 for the tangential component and 0.61 for the component perpendicular to the bank depth line.

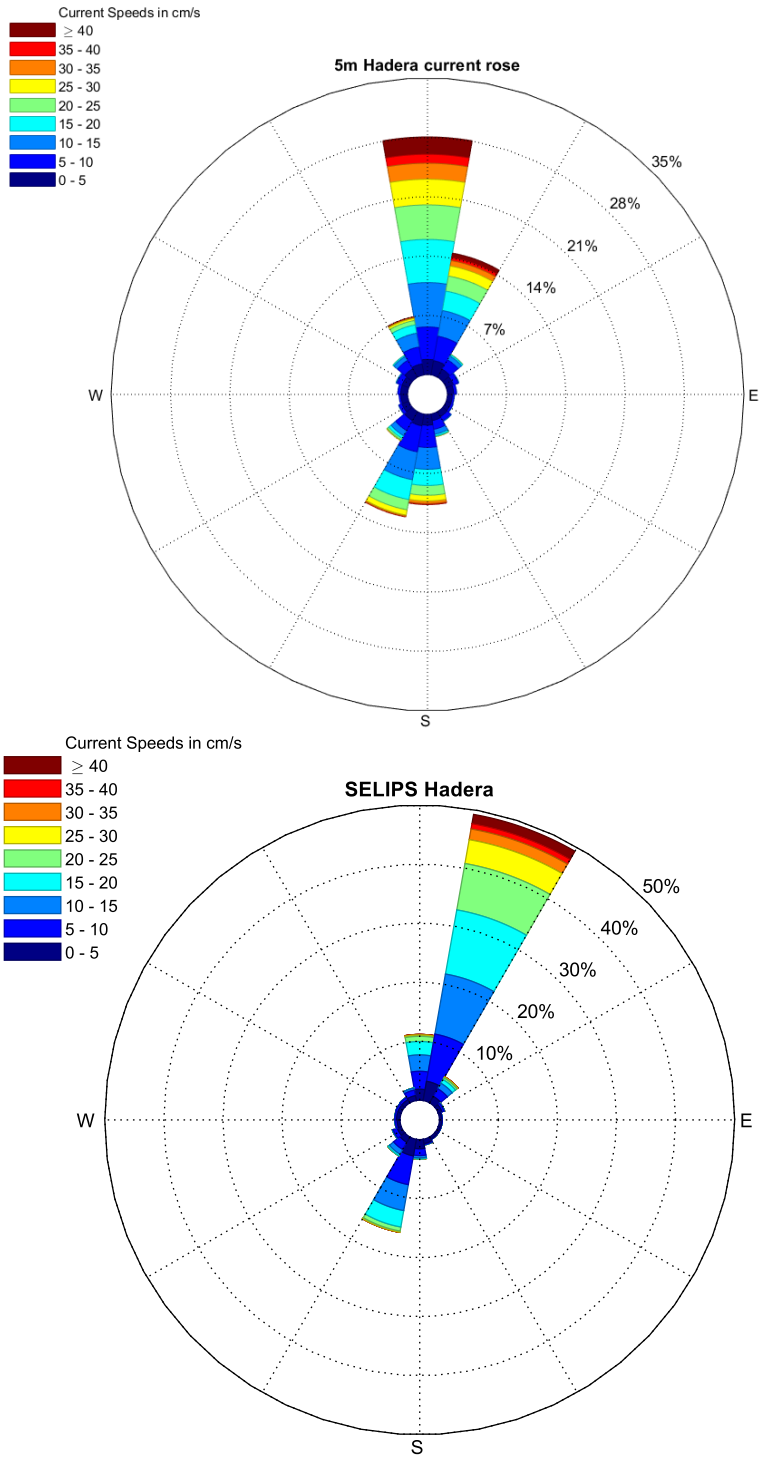

Figure A10. Rose diagrams as calculated based on the measurements in Hadera at a depth of 5 m (top) for the years 2017-2021 against the results of the SELIPS model in the same location (bottom).

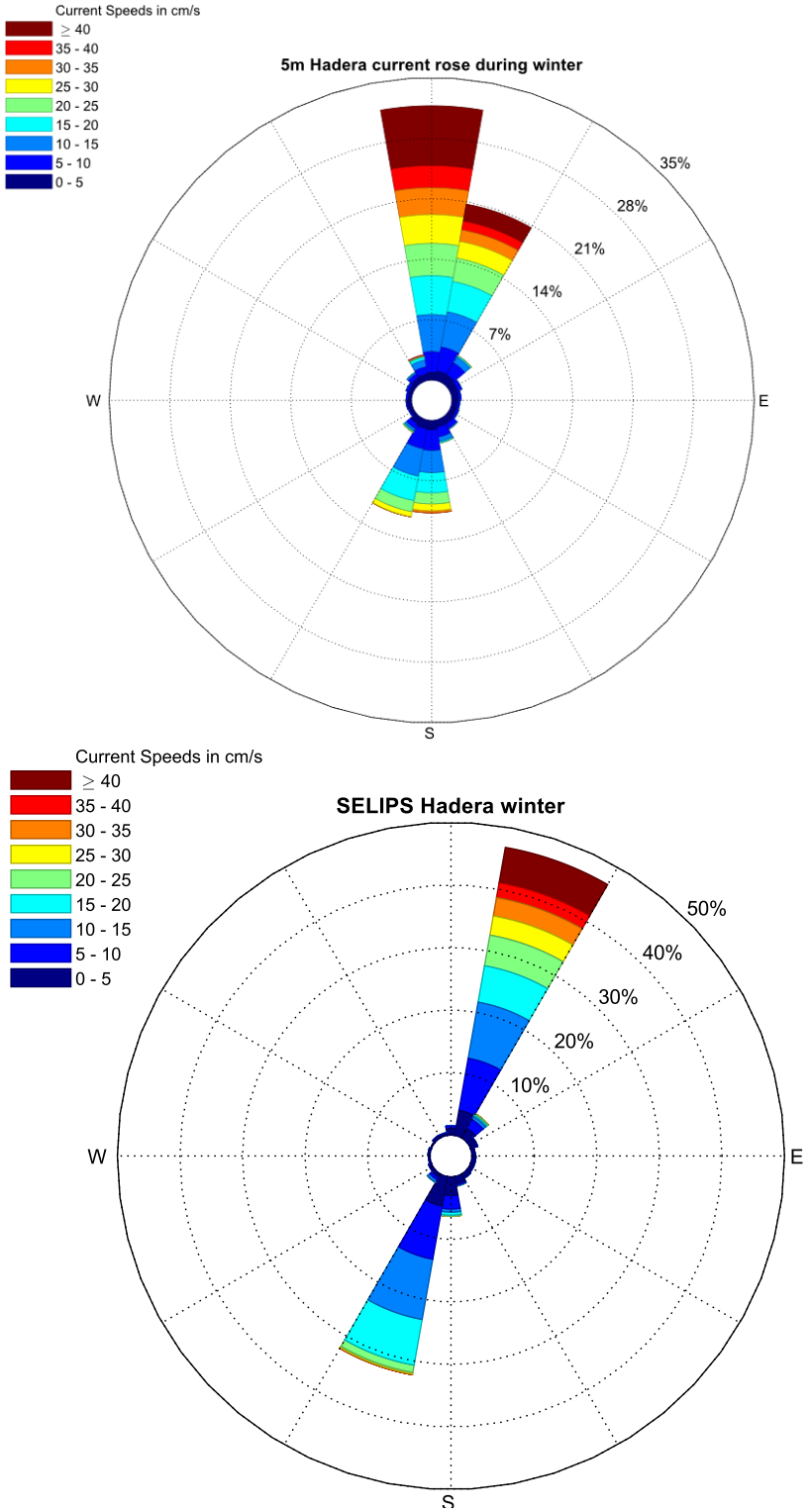

Figure A11. Lily streams as calculated based on the measurements in Hadera at a depth of 5 m (top) in the winters of 2017-2021 against the results of the SELIPS model in the same location (bottom).

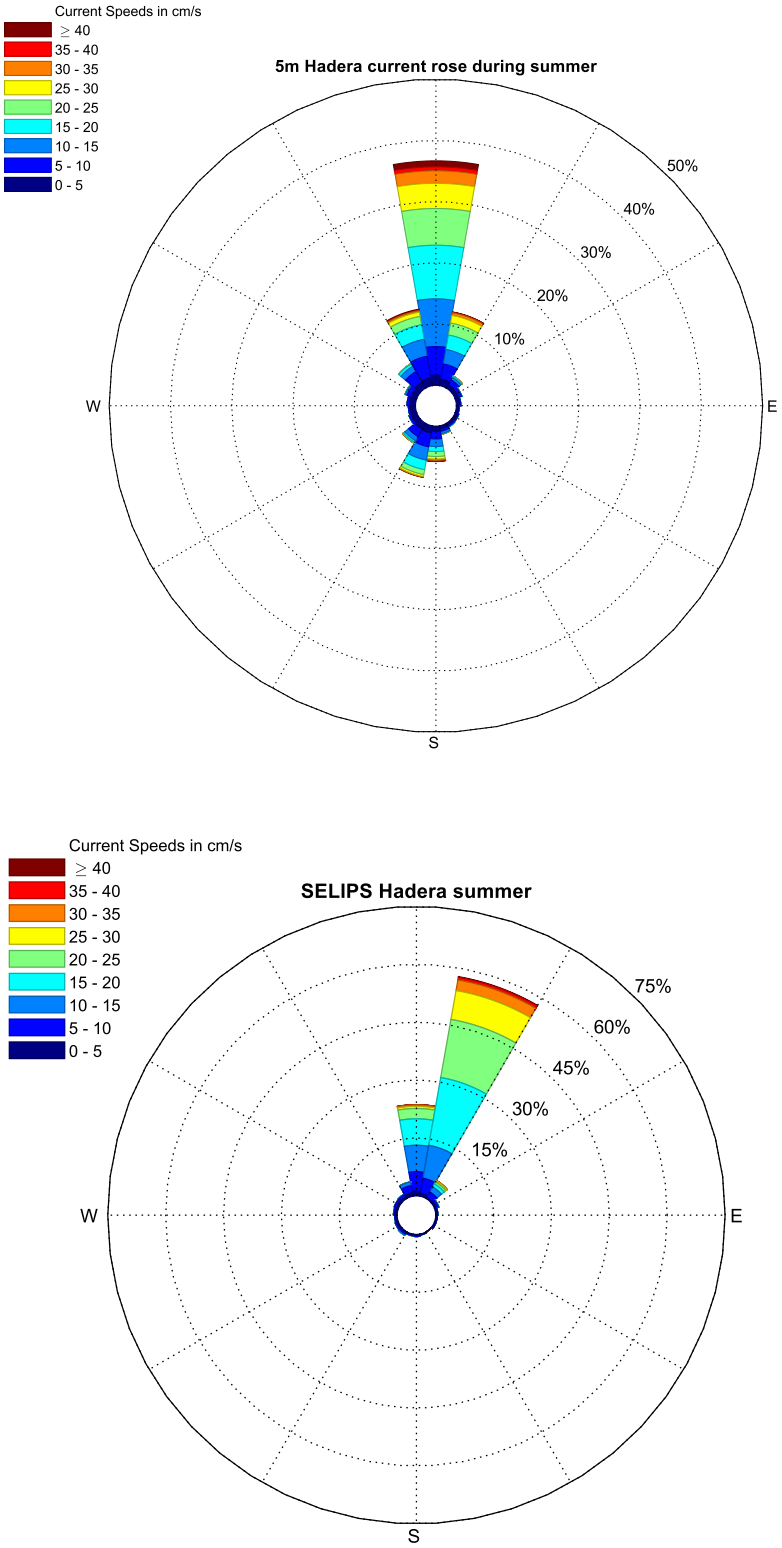

Figure A12. Rose diagrams as calculated based on the measurements in Hadera at a depth of 5 m (top) in the summers of 2017-2021 against the results of the SELIPS model in the same location (bottom).

The comparison with the DEEPLEV deep sea sampling station

DEEPLEV is a marine monitoring station located in the open sea (32° 59′ 58.2000" N, 34° 29′ 58.8120" E) about 50 km off the northern coast of Israel, where data on sea currents and hydrographic conditions are collected along the water column. The results of the model were compared with the temperature data measured at a depth of 30 meters, and with the data of the currents measured at a depth of 50 meters. All observations were proposed every three hours in order to coincide with the times of the model results. In general, a good comparison is obtained between the results of the model and the temperature values measured at a depth of 30, although there is an underestimation of the hot temperatures in the summer season (Figure A13). A comparison of the anemones of the currents at a depth of 50 meters shows that statistically the model manages to model the general movement towards the north, but the movement towards it east and south is less dominant than those observed. The flow velocity in the model is slightly lower than the measured flow in all directions (Figure A14).

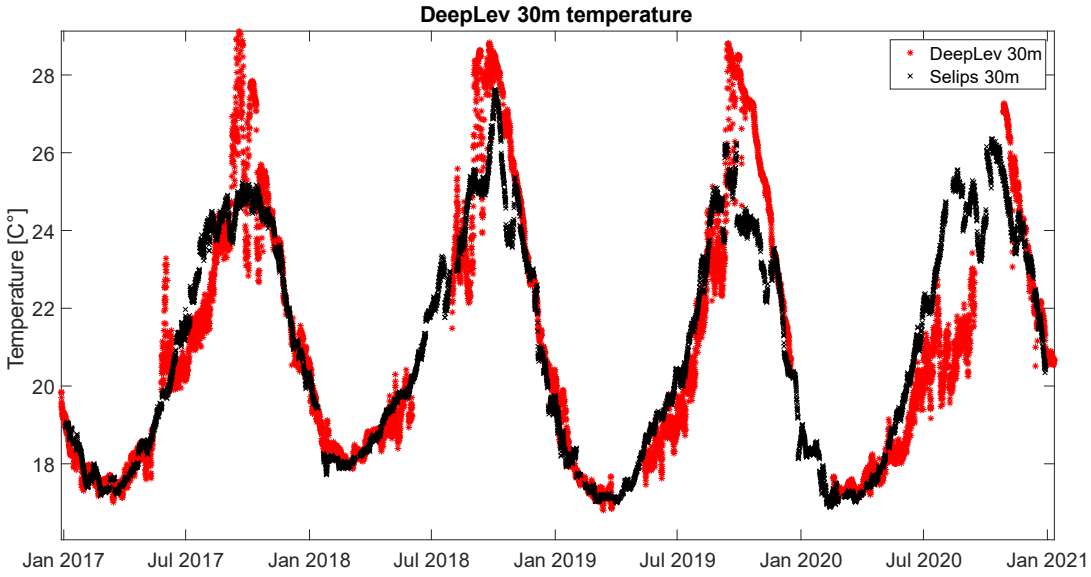

Figure A13: Averages three hours of temperature as measured at the DEEPLEV measuring station at a water depth of 30 m (red) against the results of the SELIPS model in the same position (black). The calculated correlation coefficient between the two time series is 0.9 1 with an RMSE of 1.38°C.

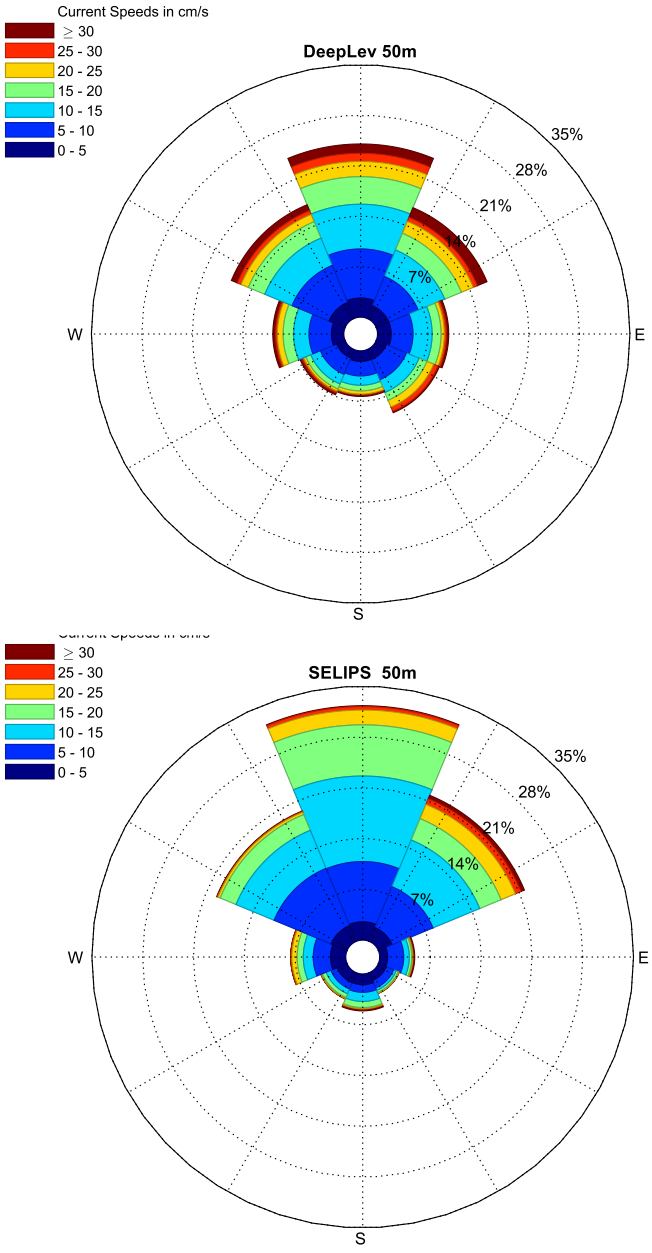

Figure A14. Rose diagram as calculated based on the measurements at the DEEPLEV deep sea sampling station at a depth of 50 m (top) against the results of the SELIPS model in the same location (bottom).

Annex 2. Parameter sensitivity test

To assess the robustness of our model results, we performed a comprehensive sensitivity test by introducing variability and modifying key parameters, as outlined in Table B1. Specifically, In this section, we detail the differences in parameterization between the main simulation and the sensitivity test conducted for this study. The adjustments made for the sensitivity test are essential for exploring the robustness of the model and understanding the potential impacts of varying parameters on the simulation outcomes. Note that due to technical and computational limitations, the pollution site Tamar was not included in the sensitivity test analysis.

For the release location, the main simulation fixed the spill site to a radius of 50 meters from the exact location of the spill. In contrast, the sensitivity test allowed for a random distance of up to 10 kilometers from the original location. This modification aims to assess how significant deviations from the expected release point might influence the overall impact of the spill on the environment.

Regarding hydrocarbon types, the main simulation utilized Erawan Condensate (liquid gas phase), Shell Oil, and Generic Medium Crude. However, the sensitivity test expanded the range of condensates included, consisting of several specific types: Algerian Condensate, Citgo, Arun Condensate, Shell Oil, various Erawan Condensate variants, and additional condensates such as Fogelberg and Martin Linge. For crude oil, the sensitivity test incorporated a broader selection that included Nigerian Medium, Tia Juana Medium, and Basrah Medium, among others. This diversification of hydrocarbon types in the sensitivity test helps to evaluate their respective behaviors and implications in oil spill scenarios.

The horizontal diffusivity parameter maintained consistency across both simulations, with the current uncertainty set at 0.05 (5%). However, in the sensitivity test, an additional horizontal diffusivity value of 1 m^2/s was introduced. This adjustment is intended to explore how different rates of diffusion can affect the dispersion of hydrocarbons in the water column.

Finally, the current field parameter differed between the two simulations. The main simulation utilized a nested model comprising both SELIPS (inner) and CMEMS (outer) models to effectively capture the intricacies of the current dynamics. In contrast, the sensitivity test

employed only the CMEMS model (outer), simplifying the current field's representation. This change serves to evaluate the effects of a less complex modeling framework on the simulation outcomes.

Comparing the ranking matrices of the original and noisy versions shows that the rankings of coastal assets remain unchanged, while some reorder occurs among offshore assets. Notably, E54 and E65 consistently exhibit the highest impact in both analyses (Figure B1). Examining the differences between the main scenario and the sensitivity analysis highlights the extent of variation introduced by the modified parameters (Figure B2).

Analyzing the results for specific metrics reveals that the separation between crude oil and condensate becomes less pronounced in the sensitivity analysis. Additionally, the differences between Zone E and Zones G, H, and I are less distinct, although the overall trends remain consistent. The summer scenario consistently exhibits the highest values across all metrics, emphasizing the seasonal influence on the results (Figs. B3–B5).

Table B1. **Parameters Modified in the Sensitivity Test Compared to the Main Simulation.** This table outlines the key differences in parameterization, including changes in release location, hydrocarbon types, horizontal diffusivity, and the current field model used for each simulation.

Parameter	Main simulation	Sensitivity test
Release location	Radius of 50 m from the exact location of the spill site.	A random distance of up to 10 km from the original location.
Hydrocarbon types	Erawan Condensate (liquid gas phase), Shell Oil and Generic Medium Crude (crude oil)	Condensates: 'ALGERIAN CONDENSATE, CITGO', 'ARUN CONDENSATE, SHELL OIL', 'EC 195-CONDENSATE, PHILLIPS','ERAWAN CONDENSATE, SHELL OIL', 'FOGELBERG CONDENSATE 2021', 'IRIS CONDENSATE 2020', 'MAIN PASS 49 CONDENSATE, SHELL OIL', 'MARTIN LINGE CONDENSATE 2016'Generic Medium Crude:'GENERIC MEDIUM CRUDE', 'NIGERIAN MEDIUM', 'TIA JUANA MEDIUM', 'LARG TRECO MEDIUM, CITGO', 'FLUID CATALYTIC CRACKER MEDIUM CYCLE OIL', 'FCC MEDIUM CYCLE OIL', 'BONNY MEDIUM, AMOCO', 'BASRAH MEDIUM'
Horizonal diffusivity	Current uncertainty = 0.05 (5%)	- Current uncertainty = 0.05 (5%) - Horizontal diffusivity= 1 m^2/s
Current field	Nested model: SELIPS (inner) + CMEMS (outer)	CMEMS (outer)

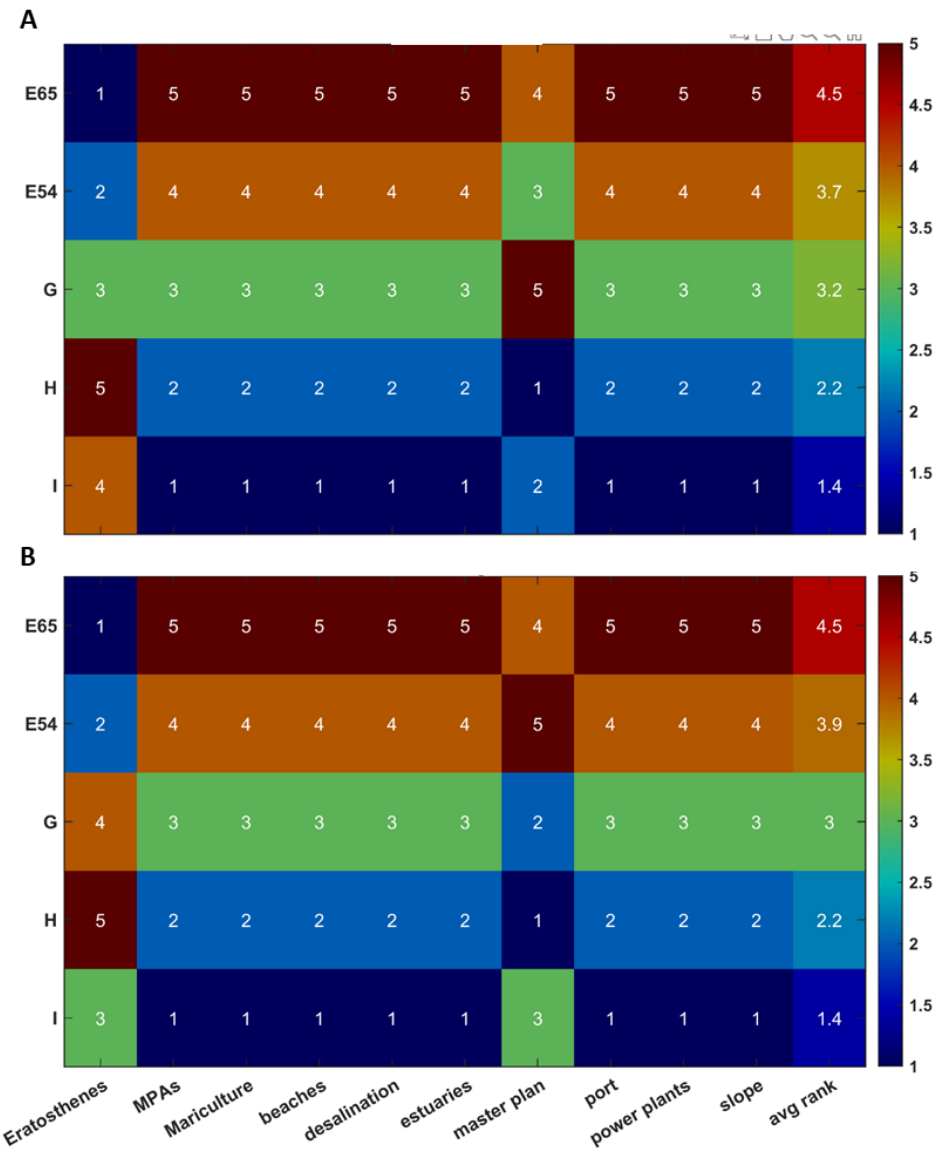

Figure B1: A comparison between main (A) and sensitivity runs (B) summary matrices representing the overall effects of the different spill sites on the different assets, ranked by the average oil mass reaching the different assets' polygons.

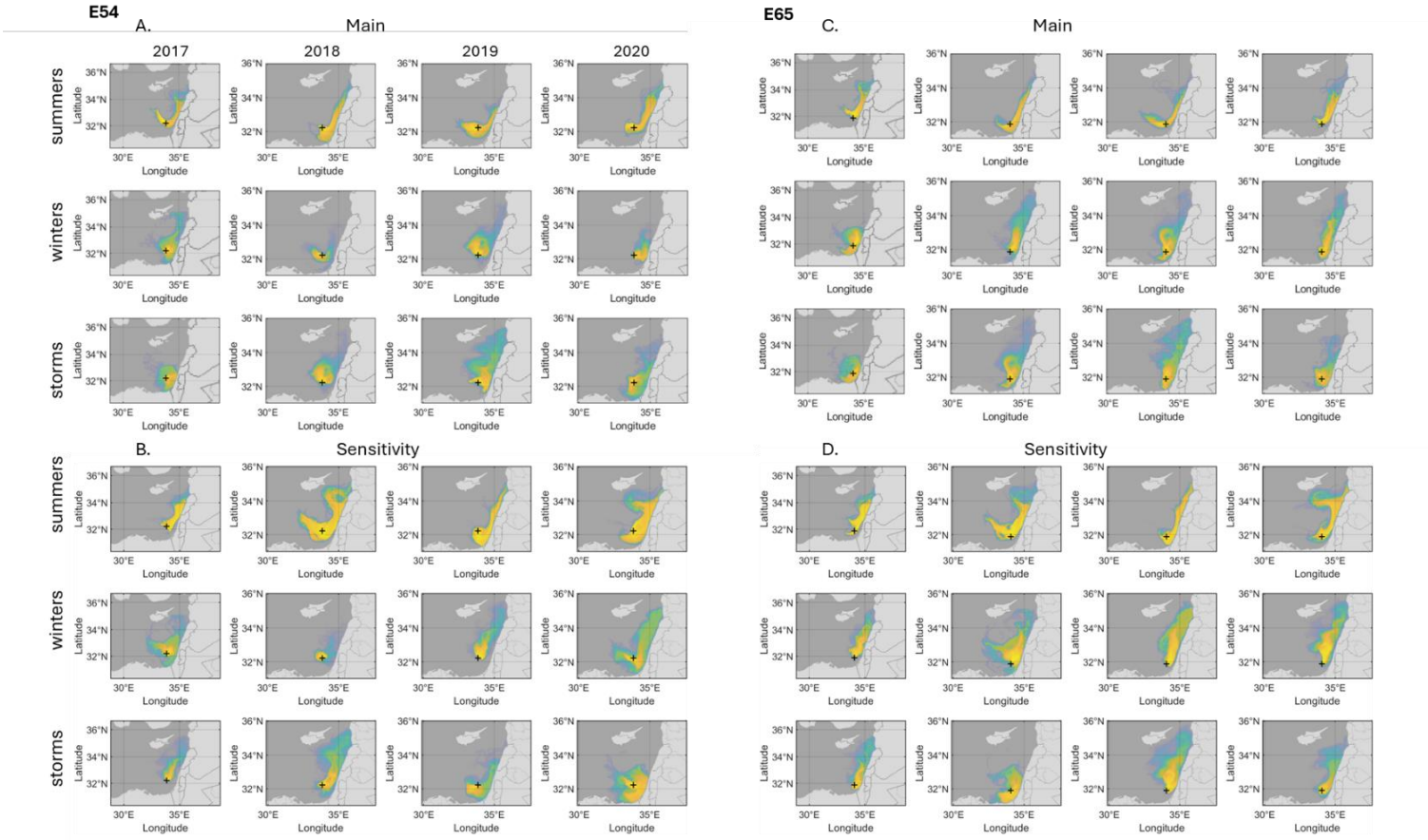

Figure B2: Total hydrocarbon concentration (ppb loglog transformed) in spills from Block E zone 54 (left panels) and 65 (right panels) for the 12 different scenarios (four years and three seasons/durations) comparing main simulation (top panels) with sensitivity runs simulations (bottom panels). The figures show variability among scenarios but similar trends within seasons, as well as variability and similarity comparing between main and sensitivity runs.

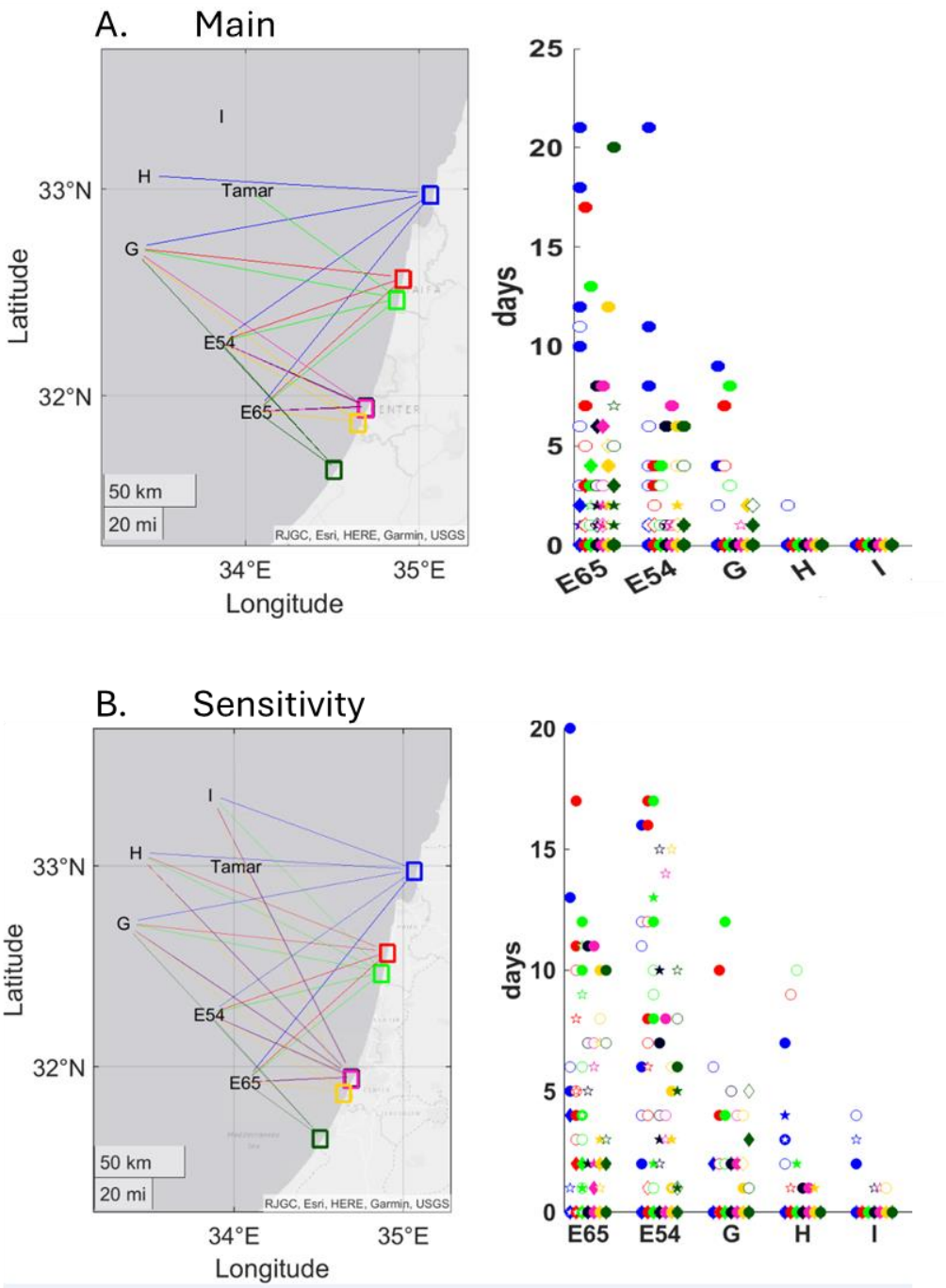

Figure B3: Comparison of our results to a sensitivity test version of the number of days in which each desalination station was exposed to hydrocarbons concentration of above 500 ppb. The trends are preserved and the differences among sites in the sensitivity test version is less significant. Note that the assets are all located east to the spill sites. For technical reasons Tamar was omitted from the sensitivity test version.

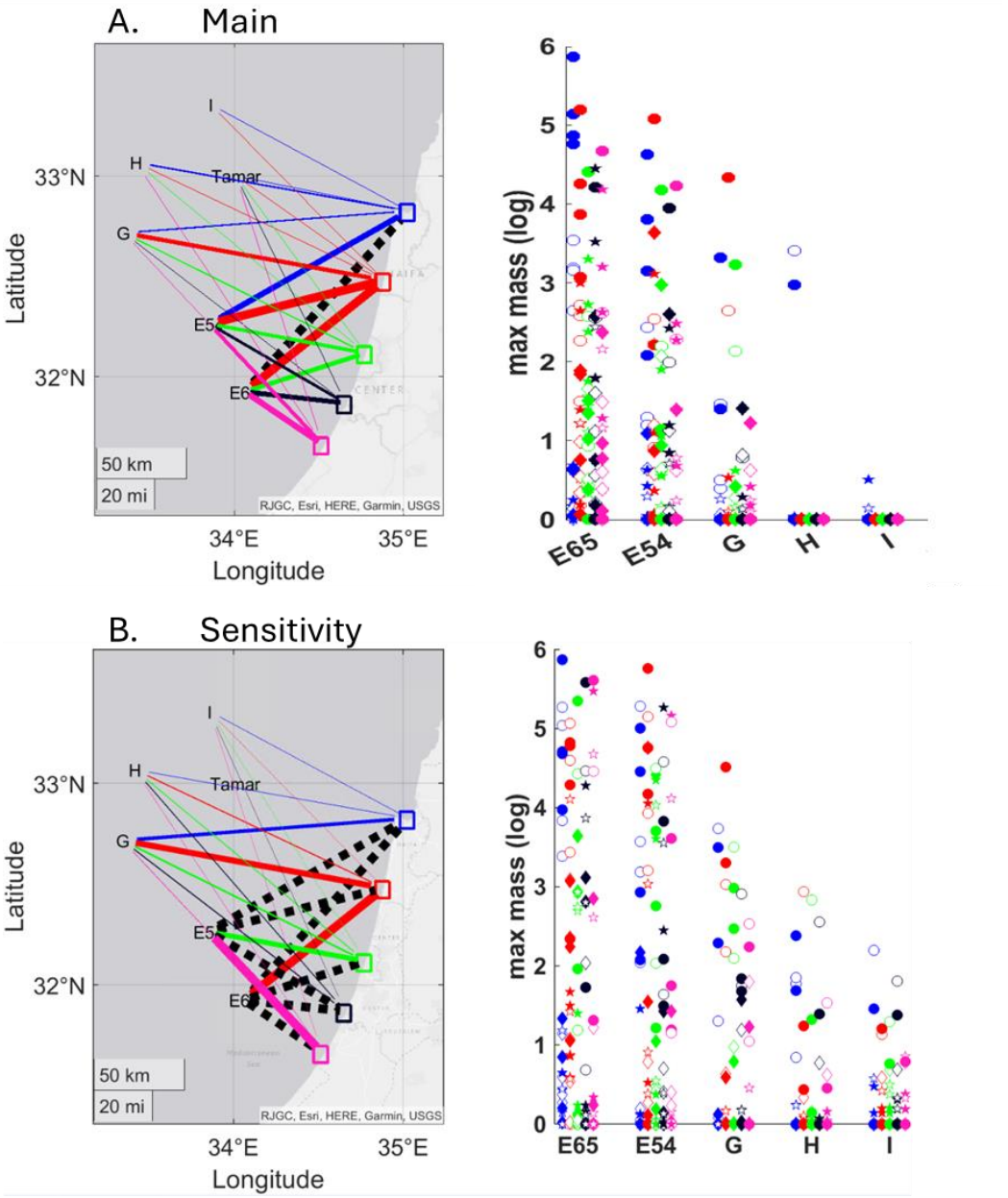

Figure B4: Comparison of our results to a sensitivity test version of the maximal mass (log(kg)) that arrived at the different power plants. The trends are preserved and the differences among sites in the sensitivity test version is less significant. Note that the assets are all located east to the spill sites. For technical reasons Tamar was omitted from the sensitivity test version.

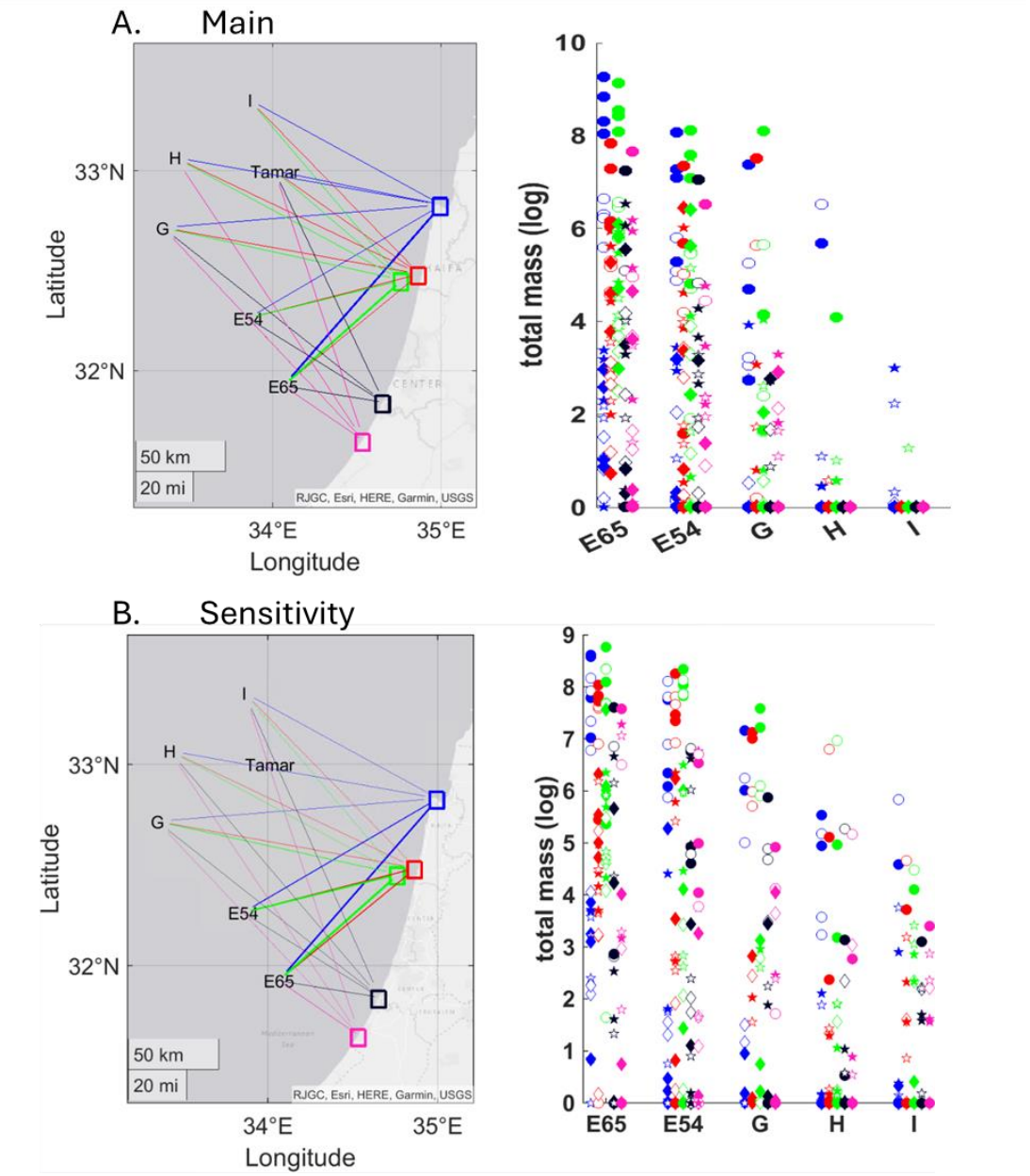

Figure B5: Comparison of our results to a sensitivity test version of the total mass that arrived at the different the different ports. The trends are preserved and the differences among sites in the sensitivity test version is less significant. Note that the assets are all located east to the spill sites. For technical reasons Tamar was omitted from the sensitivity test version.

Annex 3 – Comparison between liquid gas phase and crude oil

The spatial extent of the liquid gas phase and crude oil are highly similar between the two types of pollutants, with slightly smaller extents of the liquid gas phase due to a more rapid evaporation (Figure C1).

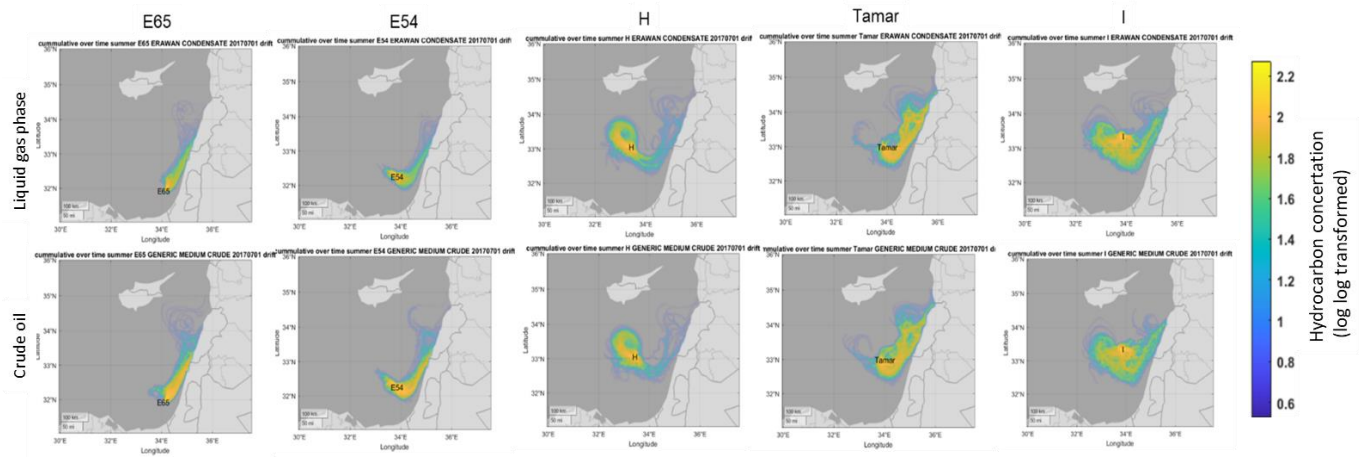

Figure C1. Simulations of liquid gas phase and crude oil for summer 2017 scenario across all pollution sites.